A quantum statistical model of a three-dimensional linear rigid rotator in a bath of oscillators: III. DC field dielectric property dynamics

1997 J. Phys. A: Math. Gen. 30 6347

(http://iopscience.iop.org/0305-4470/30/18/016)

J. Phys. A: Math. Gen. **30** (1997) 6347–6370. Printed in the UK PII: S0305-4470(97)78350-1

A quantum statistical model of a three-dimensional linear rigid rotator in a bath of oscillators: III. DC field dielectric property dynamics

J T Titantah and M N Hounkonnou†

Unité de Recherche en Physique Théorique, Institut de Mathématiques et de Sciences Physiques, BP 613 Porto-Novo, Republic of Benin

Received 26 September 1996, in final form 28 April 1997

Abstract. With the aid of a recently derived master equation, which for commodity purposes will be referred to as the Hounkonnou–Navez master equation, the dielectric properties of a polar fluid in a constant electric field regime is analysed by studying the rotational motions of the system of molecules of the dielectric medium which are assimilated to linear rigid rotators. Master equations are given for well defined matrix elements $\sigma_{l,l+1}(t)$, $\varphi_{l,l}(t)$ and $\eta_{l,l+2}(t)$. While the electrical susceptibility describes low-energy rotational transitions, the Kerr effect involves both low- and higher-energy transitions. For the quantum electrical susceptibility, the linear response limit is considered while the Kerr effect accounts for higher-order electric field effects. The classical Brownian limit of the quantum equations recover most results published to date. The convergence of the classical results (which are in the form of continued fractions) are guaranteed for large friction and/or small inertia; and low frequencies. Quantum expressions, valid for weak coupling (small friction and/or large inertia) are obtained via a rigorous mathematical theorem on weak coupling. They are the Van Vleck–Weisskopf line forms for the electrical susceptibility and the Kerr function. More importantly, explicit expressions are given for the frequency shifts and line widths. We demonstrate the transition from quantum to classical effects as the the friction/inertia parameter (ζ/I) increases. A temperature-dependent cross-over is found.

1. Introduction

To understand molecular spectra better, the investigation of molecular dynamics is indispensable. Although much work has been done to give the theoretical description of the spectra of fluids, few have successfully formulated an analytical description of absorption spectra over a wide range of temperatures and frequencies. Most of the theories are based on phenomenological models that yield parameter-dependent results.

Progress in the theory of dielectrics has been greatly motivated by the development of two statistical mechanics methods: (i) the kinetic equation method [1] and (ii) the autocorrelation function (ACF) method [2]. The former is based on developing and solving kinetic equations for the one particle probability function $f(t; \boldsymbol{r}, \boldsymbol{p})$ (or density operator $\hat{\rho}(t; \hat{\boldsymbol{r}}, \hat{\boldsymbol{p}})$) of molecules in phase space (or in the Hilbert space of the molecular dynamical variables), while the ACF method, for the electric susceptibility, is based on the Kubo linear response theory [3]. A wide range of models [4–7] use the ACF method, each differing from the other in the interpretation of the changes of the physical characteristics of motion

† To whom correspondence should be adressed.

0305-4470/97/186347+24$19.50

(momentum, orientation and energy) of the molecules as a result of collision. For the $\boldsymbol{J}$ diffusion model [2, 8], for example, the molecular orientation is unaltered after impact, while the magnitude and direction of the angular momentum are changed.

Recently [9], we presented the analysis of the Kerr effect relaxation of a system of polar linear rigid rotators in interaction with a bath of harmonic oscillators. We did this by using a master equation that we derived [10] for quantum systems. In the present work, we use this equation to calculate the electrical susceptibility and Kerr function for the case where a constant unidirectional electric field is suddenly applied to the system. This problem was classically tackled by Morita and Watanabe [11], using the rotational Smoluchowski equation. Kalmykov and Titov [2] presented a semiclassical method based on the $\boldsymbol{J}$ diffusion model. Their analysis was limited to the electrical susceptibility calculation. In the same paper, they used the ACF method on the Van Vleck–Weisskopf model. This model supposes that, after every collision, the molecule can be found in any possible state with the probability proportional to the Boltzmann distribution corresponding to the instantaneous Hamiltonian of the system. Their results could be recovered from the results we obtain in this work for the weak coupling or the rotating wave approximation limit (RWA). The classical theories enumerated above together with our recent works [12, 13] effectively describe the high-density spectra of polar fluids.

This paper is organized as follows. In section 2, a brief description of the model is given together with the Hounkonnou–Navez (HN) master equation governing the evolution of the probability density operator of the rotator. In section 3, master equations are given for some well defined matrix elements. In section 4, the electrical susceptibility and Kerr function are calculated for the classical Brownian limit. In section 5, the RWA limit is considered. In section 6, we finish the paper with discussions.

2. Description of the model

We consider a linear rigid rotator, fixed at its centre and free to rotate about the latter. It interacts with a bath of harmonic oscillators. The rotator-bath system Hilbert space H is the tensor product of the rotator H_S and bath H_B Hilbert spaces, respectively:

$$H = H_S \otimes H_B. \tag{1}$$

The Hamiltonian of the system subjected to an applied electric field is

$$\hat{H}_T(t) = \hat{H} + \hat{H}_E(t) \tag{2}$$

where $\hat{H}$ is the Hamiltonian used in [9, 10] and

$$\hat{H}_E(t) = \begin{cases} 0 & \text{if } t \leqslant 0 \\ -\mu E \cos\hat{\beta} - \dfrac{\alpha_\parallel - \alpha_\perp}{2} E^2 \cos^2\hat{\beta} - \dfrac{\alpha_\perp}{2} E^2 \hat{I} & \text{if } t > 0. \end{cases} \tag{3}$$

$\alpha_\parallel$ and $\alpha_\perp$ are, respectively, the rotator polarizability tensor components parallel and perpendicular to the molecular principal axis. We assume that the electric field is applied along the z-axis of the laboratory frame. $\hat{\beta}$ is the polar angle or the angle between the applied field and the principal axis of the rotator.

The evolution of the reduced probability density operator $\hat{\rho}_S(t)$ is governed by the HN master equation [9, 10]

$$\frac{\partial\hat{\rho}_S(t)}{\partial t} + \frac{\mathrm{i}}{\hbar}[\hat{H}_S, \hat{\rho}_S(t)] + \hat{K}\hat{\rho}_S(t) = -\frac{\mathrm{i}}{\hbar}[\hat{H}_E, \hat{\rho}_S(t)] \tag{4}$$

with the collision term

$$\hat{K}\hat{\rho}(t) = \frac{\zeta}{I}\sum_{l=1}^{\infty} l\{A_l^*\hat{\boldsymbol{u}}\cdot\hat{\boldsymbol{u}}_l^-\hat{\rho}_S(t) - A_l\hat{\boldsymbol{u}}\cdot\hat{\rho}_S(t)\hat{\boldsymbol{u}}_l^+ + B_l\hat{\boldsymbol{u}}\cdot\hat{\boldsymbol{u}}_l^+\hat{\rho}_S(t) - B_l^*\hat{\boldsymbol{u}}\cdot\hat{\rho}_S(t)\hat{\boldsymbol{u}}_l^- - A_l^*\hat{\boldsymbol{u}}_l^-\cdot\hat{\rho}_S(t)\hat{\boldsymbol{u}} + A_l\hat{\rho}_S(t)\hat{\boldsymbol{u}}_l^+\cdot\hat{\boldsymbol{u}} + B_l^*\hat{\rho}_S(t)\hat{\boldsymbol{u}}_l^-\cdot\hat{\boldsymbol{u}} - B_l\hat{\boldsymbol{u}}_l^+\hat{\rho}_S(t)\cdot\hat{\boldsymbol{u}}\} \tag{5}$$

where

$$A_l = \frac{\omega_D^2}{\omega_D^2+\omega_l^2}\left[1 + N(\omega_l) + \mathrm{i}\left(\kappa(x_l,x_D) - \frac{\omega_l}{2\omega_D}\right)\right] \tag{6}$$

$$B_l = \frac{\omega_D^2}{\omega_D^2+\omega_l^2}\left[N(\omega_l) + \mathrm{i}\left(\kappa(x_l,x_D) + \frac{\omega_l}{2\omega_D}\right)\right] \tag{7}$$

with

$$\kappa(x_l,x_D) = -\left[\frac{1}{x_D} + 2\sum_{n=1}^{\infty}\frac{x_l^2 - 2\pi x_D n}{(x_l+x_D)(x_l^2+4\pi^2n^2)}\right] \tag{8}$$

and

$$x_D = \beta\hbar\omega_D \qquad x_l = \beta\hbar\omega_l \qquad \beta = \frac{1}{k_BT} \qquad n = 1,2,3,\ldots \tag{9}$$

where we used the spherical harmonic expansion of the unit vector operator $\hat{\boldsymbol{u}}$ as [9, 10]

$$\hat{\boldsymbol{u}}(t) = \sum_{l=1}^{\infty}(\hat{\boldsymbol{u}}_l^+ + \hat{\boldsymbol{u}}_l^-(t)). \tag{10}$$

ω_D is the characteristic Debye frequency, k_B is the Boltzmann constant, T is the absolute temperature and $N(\omega_l)$ is the occupation number of the rotator quantum level l. A_l^* and B_l^* are the complex conjugates of A_l and B_l, respectively. ζ is the friction coefficient characterizing the effect of the bath oscillator concentration on the rotator dynamics. This equation is the same as those of [9, 10] but for the fact that there is an explicit presence of the electric field. This is because we are interested in the investigation of how a thermally equilibrated system in the the absence of any stress will relax to the new equilibrium in the presence of a stress. In other words, is the relaxation following the sudden application of a DC field explained by the same mechanism as the relaxation following its sudden removal?

An appropriate initial condition for the above master equation is the canonical probability density operator in the absence of the electric field.

If $Q(t)$ is the heat gained by the rotator from the bath and as a result of the work done by the electric field on the dipole through the interaction with the dipole moment $\boldsymbol{\mu}$, we write the energy balance equation

$$\frac{\mathrm{d}}{\mathrm{d}t}Q(t) = \frac{\mathrm{d}}{\mathrm{d}t}U(t) + \frac{\mathrm{d}}{\mathrm{d}t}W(t) \tag{11}$$

where $U(t)$, the internal energy of the rotator, and $W(t)$, the work done by the field, are defined as:

$$U(t) = \langle\hat{H}_S\hat{\rho}_S(t)\rangle \qquad \text{and} \qquad W(t) = \langle\hat{H}_E\hat{\rho}_S(t)\rangle \tag{12}$$

with the angle brackets $\langle\ldots\rangle$ denoting ensemble averaging. By using the HN master equation (4), we obtain, for a constant field,

$$\frac{\mathrm{d}}{\mathrm{d}t}Q(t) = 2B(K_BT - U(t)) + \frac{4\mu E_c}{3}\sum_{l=0}^{\infty}\frac{\overline{h}}{I}(l+1)^2\frac{\mathrm{e}^{\beta E_l}}{Z}\,\mathrm{Im}\,\sigma_{l,l+1}(t) \tag{13}$$

to second order in electric field strength. Im denotes the imaginary part, $B = (\zeta/I)$ is the rotator-bath characteristic frequency. To obtain this equation, we used the change of function,

$$\sum_{m=-l}^{l} C(l+1,m)\rho^{m}_{l,l+1}(t) = \sum_{m=-l}^{l} C(l+1,m)^2\sigma_{l,l+1}(t)\frac{\mathrm{e}^{-\beta E_l}}{Z} \tag{14}$$

where Z is the free rotator partition function; $E_l = (\hbar^2/2I)l(l+1)$ is the rotator rotational kinetic energy and $C(l,m) = \sqrt{\frac{(l-m)(l+m)}{(2l-1)(2l+1)}}$.

$\sigma_{l,l+1}(t)$ is independent of m. The matrix elements $\rho^{m}_{l,l'}(t)$ are defined as

$$\rho^{m}_{l,l'}(t) = \langle l,m|\hat{\rho}_S(t)|l',m\rangle. \tag{15}$$

Remark that in the absence of the field $Q = U$ and the internal energy of the rotator tends asymptotically to that of the thermal bath. The energy balance equation is very important as it describes well the process of energy transfer from the bath to the rotator or vice versa. The matrix elements $\sigma_{l,l+1}(t)$ determine explicitly the electric susceptibility; the latter, thus, plays a vital role in the energy transfer processes.

3. Master equations for matrix elements

We want to calculate the electric polarization $P(t)$ defined as the ensemble average of the component of the rotator dipole moment parallel to the applied electric field which we assume directed along the z-axis of the laboratory frame [1, 12–14]

$$P(t) = \sum_{l=0}^{\infty}\sum_{m=-l}^{l}\langle l,m|\hat{\mu}_z\hat{\rho}_S(t)|l,m\rangle \tag{16}$$

where $\hat{\mu}_z = \mu\hat{u}_z$, with $\hat{u}_z$ being the z component of the rotator orientation operator. By using the spherical harmonic representation of $\hat{u}_z$, we obtain

$$P(t) = \frac{2\mu}{3}\sum_{l=0}^{\infty}(l+1)\frac{\mathrm{e}^{-\beta E_l}}{Z}\,\mathrm{Re}\,\sigma_{l,l+1}(t) \tag{17}$$

where Z is the one-particle free rotator canonical partition function and Re denotes the real part.

The Kerr function is the ensemble average of the second-order Legendre polynomial $P_2(\cos\beta)$ [1, 12–14]

$$\Phi(t) = \frac{1}{2}\sum_{l=0}^{\infty}\sum_{m=-l}^{l}\langle l,m|(3\hat{u}_z^2-1)\hat{\rho}_S(t)|l,m\rangle. \tag{18}$$

On defining matrix elements $\varphi_{l,l}$ and $\eta_{l,l+2}$ through

$$\sum_{m=-l}^{l}\frac{l(l+1)-3m^2}{(2l-1)(2l+3)}\langle l,m|\hat{\rho}_S(t)|l,m\rangle = \frac{2}{15}\frac{\mathrm{e}^{-\beta E_l}}{Z}\frac{l(l+1)(2l+1)}{(2l-1)(2l+3)}\varphi_{l,l}(t) \tag{19}$$

and

$$\sum_{m=-l}^{l}\sqrt{\frac{((l+1)^2-m^2)((l+2)^2-m^2)}{(2l+1)(2l+3)^2(2l+5)}}\langle l,m|\hat{\rho}_S(t)|l+2,m\rangle$$
$$= \sum_{m=-l}^{l}\frac{((l+1)^2-m^2)((l+2)^2-m^2)}{(2l+1)(2l+3)^2(2l+5)}\frac{\mathrm{e}^{-\beta E_l}}{Z}\eta_{l,l+2}(t) \tag{20}$$

we obtain,

$$\Phi(t) = \frac{2}{15}\sum_{l=0}^{\infty}\frac{\mathrm{e}^{-\beta E_l}}{Z}\frac{(l+1)}{(2l+3)}\left\{\frac{l(2l+1)}{(2l-1)}\varphi_{l,l}(t) + 3(l+2)\,\mathrm{Re}\,\eta_{l,l+2}(t)\right\}. \tag{21}$$

We now give the master equations verified by the different matrix elements $\sigma_{l,l+1}$, $\varphi_{l,l}(t)$ and $\eta_{l,l+2}(t)$.

To obtain the equation verified by $\sigma_{l,l+1}$, we multiply through the HN master equation (4) from the left by $\sum_{m=-l}^{l} C(l+1,m)|l+1,m\rangle\langle l,m|$ and take trace. This leads to

$$\begin{aligned}
&\sum_{m=-l}^{l}\frac{1}{Z}\Bigg[C(l+1,m)^2\mathrm{e}^{-\beta E_l}\left(\frac{\partial}{\partial t} - \frac{\mathrm{i}\overline{h}}{I}(l+1)\right)\sigma_{l,l+1}(t)\\
&\qquad + B\Bigg\{C(l+1,m)^2\mathrm{e}^{-\beta E_l}\Bigg[(A_l^* l^2 + B_{l+1}(l+1)^2)\frac{1}{2l+1} + (A_{l+1}(l+1)^2\\
&\qquad + B_{l+2}^*(l+2)^2)\frac{1}{2l+3}\Bigg]\sigma_{l,l+1}(t)\\
&\qquad - C(l,m)^2\mathrm{e}^{-\beta E_{l-1}}\frac{l+1}{2l+1}[(B_l l + (l+1)B_{l+1}^*]\sigma_{l-1,l}(t)(1-\delta_{lo})\\
&\qquad - C(l+2,m)^2\mathrm{e}^{-\beta E_{l+1}}\frac{l+1}{2l+3}[A_{l+1}^*(l+1) + A_{l+2}(l+2)]\sigma_{l+1,l+2}(t)\\
&\qquad - C(l+1,m)^2\frac{l+1}{(2l+1)(2l+3)}[A_{l+1}^*(l+1) + B_{l+1}^*(l+1)]\sigma_{l,l+1}^*(t)\Bigg\}\Bigg]\\
&= \mathrm{i}\sum_{m=-l}^{l}\Bigg[\frac{\mu E(t)}{\overline{h}}\Bigg\{C(l+1,m)^2(\rho_{l+1,l+1}^m - \rho_{l,l}^m)\\
&\qquad + C(l,m)^2C(l+1,m)^2\frac{\mathrm{e}^{-\beta E_{l-1}}}{Z}\eta_{l-1,l+1}(t)(1-\delta_{l,0})\\
&\qquad - C(l+1,m)^2C(l+2,m)^2\frac{\mathrm{e}^{-\beta E_l}}{Z}\eta_{l,l+2}(t)\Bigg\}\\
&\qquad + \frac{\Delta\alpha E(t)^2}{2\overline{h}}\Bigg\{[C(l,m)^2 - C(l+2,m)^2]C(l+1,m)^2\frac{\mathrm{e}^{-\beta E_l}}{Z}\sigma_{l,l+1}(t)\\
&\qquad - C(l,m)^2C(l+1,m)^2\frac{\mathrm{e}^{-\beta E_{l-1}}}{Z}\sigma_{l-1,l}(t)(1-\delta_{l,0})\\
&\qquad + C(l-1,m)^2C(l,m)^2C(l+1,m)^2\frac{\mathrm{e}^{-\beta E_{l-2}}}{Z}\lambda_{l-2,l+1}(t)(1-\delta_{l,0})(1-\delta_{l,1})\\
&\qquad - C(l+1,m)^2C(l+2,m)^2C(l+3,m)^2\frac{\mathrm{e}^{-\beta E_l}}{Z}\lambda_{l,l+3}(t)\\
&\qquad + C(l+1,m)^2C(l+2,m)^2\frac{\mathrm{e}^{-\beta E_{l+1}}}{Z}\sigma_{l+1,l+2}(t)\Bigg\}\Bigg].
\end{aligned} \tag{22}$$

The equation for $\varphi_{l,l}$ is obtained by multiplying through the master equation by $\{(l(l+1)-3m^2)/(2l-1)(2l+3)\}|l,m\rangle\langle l,m|$ and taking trace to obtain

$$\begin{aligned}
&\sum_{m=-l}^{l}\Bigg[\frac{\partial}{\partial t}\frac{l(l+1)-3m^2}{(2l-1)(2l+3)}\rho_{l,l}^m(t) + 2B\,\mathrm{Re}\left\{\frac{[A_l l^2 + B_{l+1}(l+1)^2]}{2l+1}\frac{l(l+1)-3m^2}{(2l-1)(2l+3)}\rho_{l,l}^m(t)\right.\\
&\qquad \left. - A_{l+1}l\frac{(l+1)(l+2)-3m^2}{(2l+1)(2l+3)^2}\rho_{l+1,l+1}^m(t)\right.
\end{aligned}$$

$$
\begin{aligned}
&-B_l l\frac{l(l-1)-3m^2}{(2l-1)^2(2l+3)}\rho^m_{l-1,l-1}(t)(1-\delta_{l0})\\
&-3\frac{[B_l l+A_{l+1}(l+1)]}{(2l+1)(2l+3)}C(l,m)^2C(l+1,m)^2\frac{\mathrm{e}^{-\beta E_{l-1}}}{Z}\eta_{l-1,l+1}(t)(1-\delta_{l0})\Bigg\}\Bigg]\\
&=\frac{2}{Z}\sum_{m=-l}^{l}\frac{l(l+1)-3m^2}{(2l-1)(2l+3)}\Bigg\{\frac{\mu E(t)}{\overline{h}}\Bigg[C(l+1,m)^2\mathrm{e}^{-\beta E_l}\,\mathrm{Im}\,\sigma_{l,l+1}(t)-C(l,m)^2\\
&\times\frac{\mathrm{e}^{-\beta E_{l-1}}}{Z}\,\mathrm{Im}\,\sigma_{l-1,l}(t)(1-\delta_{l,0})\Bigg]\\
&+\frac{\Delta\alpha E(t)^2}{2\overline{h}}[C(l+1,m)^2C(l+1,m)^2\mathrm{e}^{-\beta E_l}\,\mathrm{Im}\,\eta_{l,l+2}(t)\\
&-C(l-1,m)^2C(l,m)^2\mathrm{e}^{-\beta E_{l-2}}\,\mathrm{Im}\,\eta_{l-2,l}(t)(1-\delta_{l,0})(1-\delta_{l,1})]\Bigg\}
\end{aligned}
\tag{23}
$$

where Im denotes the imaginary part.

Finally, the equation for $\eta_{l,l+2}$ is obtained by multiplying through the master equation (4) from the left by $\sum_{m=-l}^{l}C(l+1,m)C(l+2,m)|l+2,m\rangle\langle l,m|$ and taking trace:

$$
\begin{aligned}
&\sum_{m=-l}^{l}\Bigg[C(l+1,m)^2C(l+2,m)^2\frac{\mathrm{e}^{-\beta E_l}}{Z}\left[\frac{\partial}{\partial t}-\frac{\mathrm{i}\overline{h}}{I}(2l+3)\right]\eta_{l,l+2}(t)\\
&+B\Bigg\{C(l+1,m)^2C(l+2,m)^2\frac{\mathrm{e}^{-\beta E_l}}{Z}\Bigg\{[A_l^*l^2+B_{l+1}(l+1)^2]\frac{1}{2l+1}\\
&+[A_{l+2}(l+2)^2+B^*_{l+3}(l+3)^2]\frac{1}{2l+5}\Bigg\}\eta_{l,l+2}(t)\\
&-\frac{l+2}{2l+3}C(l,m)^2C(l+1,m)^2\frac{\mathrm{e}^{-\beta E_{l-1}}}{Z}[B_l l+B_{l+2}(l+2)]\eta_{l-1,l+1}(t)(1-\delta_{lo})\\
&-C(l+2,m)^2C(l+3,m)^2\frac{\mathrm{e}^{-\beta E_{l+1}}}{Z}\frac{l+1}{2l+3}\\
&\times[A^*_{l+1}(l+1)+A_{l+3}(l+3)]\eta_{l+1,l+3}(t)\\
&-2\frac{[A^*_{l+1}(l+1)+B_{l+2}(l+2)]}{(2l+3)^2}\frac{(l+1)(l+2)-3m^2}{(2l+1)(2l+5)}\varphi_{l+1,l+1}(t)\Bigg\}\Bigg]\\
&=\mathrm{i}\sum_{m=-l}^{l}\Bigg[\frac{\mu E(t)}{\overline{h}}\Bigg\{C(l+1,m)^2C(l+2,m)^2\frac{\mathrm{e}^{-\beta E_{l+1}}}{Z}\sigma_{l+1,l+2}(t)\\
&-C(l+1,m)^2C(l+2,m)^2\frac{\mathrm{e}^{-\beta E_l}}{Z}\sigma_{l,l+1}(t)\\
&+C(l,m)^2C(l+1,m)^2C(l+2,m)^2\frac{\mathrm{e}^{-\beta E_{l-1}}}{Z}\lambda_{l-1,l+2}(t)(1-\delta_{l,0})\\
&-C(l+1,m)^2C(l+2,m)^2(l+3,m)^2\frac{\mathrm{e}^{-\beta E_l}}{Z}\lambda_{l,l+3}(t)\Bigg\}\\
&-\frac{\Delta\alpha E(t)^2}{2\overline{h}}\Bigg\{C(l+1,m)^2C(l+2,m)^2(\rho^m_{l,l}(t)-\rho^m_{l+1,l+1}(t))\\
&-[C(l,m)^2+C(l+1,m)^2-C(l+2,m)^2C(l+3,m)^2]\\
&\times C(l+1,m)^2C(l+2,m)^2\frac{\mathrm{e}^{-\beta E_l}}{Z}\eta_{l,l+2}(t)-C(l+1,m)^2C(l+2,m)^2
\end{aligned}
$$

$$\times\left(C(l-1,m)^2C(l,m)^2\frac{\mathrm{e}^{-\beta E_{l-2}}}{Z}\zeta_{l-2,l+2}(t)(1-\delta_{l,0})(1-\delta_{l,1})\right.$$
$$\left.-C(l+3,m)^2C(l+4,m)^2\frac{\mathrm{e}^{-\beta E_l}}{Z}\zeta_{l,l+4}(t)\right)\Bigg\}\Bigg]. \tag{24}$$

The new matrix elements $\lambda_{l,l+3}(t)$ and $\zeta_{l,l+4}(t)$ are defined through

$$\begin{aligned}C(l+1,m)C(l+2,m)C(l+3,m)\langle l,m|\hat{\rho}_S(t)|l+3,m\rangle&\\ =(C(l+1,m)C(l+2,m)C(l+3,m))^2\lambda_{l,l+3}(t)C(l+1,m)C(l+2,m)&\\ \times C(l+3,m)C(l+4,m)\langle l,m|\hat{\rho}_S(t)|l+4,m\rangle&\\ =(C(l+1,m)C(l+2,m)C(l+3,m)C(l+4,m))^2\zeta_{l,l+4}(t).&\end{aligned} \tag{25}$$

The initial conditions on $\sigma_{l,l+1}(t)$, $\varphi_{l,l}(t)$ and $\eta_{l,l+2}(t)$ are

$$\sigma_{l,l+1}(t=0)=\varphi_{l,l}(t=0)=\eta_{l,l+2}(t=0)=0. \tag{26}$$

For commodity, equations (22)–(24) shall henceforth be referred to as Hounkonnou–Titantah (HT) equations for the electrical susceptibility and the Kerr effect, as they will frequently be used in subsequent works. Equation (22) will be referred as HT1, (23) as HT2 and (24) as HT3.

Remark that any matrix element $K_{l,l+n}$ (with $n\neq 0$) is at least an n-order electric field term. In particular, $\varphi_{l,l}(t)$ is a second-order term. This follows from HT1 that the polarization is an odd function of electric field strength $E(t)$. Thus, the polarization reverses as the field reverses. In contrast, the electrical birefringence is an even function of $E(t)$. The modification in the refractive index tensor is thus, independent of the field orientation. In the analysis of the electrical susceptibility, we limit ourselves to the linear response regime while the Kerr effect will be given to second order in the electric field strength. In the $\sigma_{l,l+1}(t)$ equation (HT1), we, therefore, ignore third-order terms such as $E(t)\eta_{l,l+2}(t)$ and $E(t)^2\sigma_{l,l+1}(t)$; and fifth-order terms such as $E(t)^2\lambda_{l,l+3}(t)$ while retaining first-order terms such as $E(t)\rho^m_{l,l}(t)$ in which case we consider the canonical thermal equilibrium density matrix element in zero field ($\rho^m_{l,l}(t)=(\rho^m_{l,l})^{eq}=\mathrm{e}^{-\beta E_l}/Z$). In the $\eta_{l,l+2}(t)$ (HT3) and $\varphi_{l,l}(t)$ (HT2) equations, fourth-order field terms such as $E(t)^2\eta_{l,l+2}(t)$, $E(t)\lambda_{l,l+3}(t)$ and sixth-order terms such as $E(t)^2\zeta_{l,l+4}(t)$ are ignored. The appropriate reduced HT equations are, thus:

(i) the reduced HT1:

$$\begin{aligned}\left(\frac{\partial}{\partial t}-\frac{\mathrm{i}\bar{h}}{I}(l+1)\right)\sigma_{l,l+1}(t)+B\Bigg[\Bigg\{&(A_l^*l^2+B_{l+1}(l+1)^2)\frac{1}{2l+1}+(A_{l+1}(l+1)^2\\ &+B^*_{l+2}(l+2)^2)\frac{1}{2l+3}\Bigg\}\sigma_{l,l+1}(t)\\ &-\mathrm{e}^{\beta(E_l-E_{l-1})}\frac{l}{2l+1}[B_ll+(l+1)B^*_{l+1}]\sigma_{l-1,l}(t)(1-\delta_{l0})\\ &-\mathrm{e}^{-\beta(E_{l+1}-E_l)}\frac{l+2}{2l+3}[A^*_{l+1}(l+1)+A_{l+2}(l+2)]\sigma_{l+1,l+2}(t)\\ &-\frac{l+1}{(2l+1)(2l+3)}[A^*_{l+1}(l+1)+B^*_{l+1}(l+1)]\sigma^*_{l,l+1}(t)\Bigg]\\ =&-\mathrm{i}\frac{\mu E(t)}{\bar{h}}(1-\mathrm{e}^{-\beta(E_{l+1}-E_l)})\end{aligned} \tag{27}$$

(ii) the reduced HT2:

$$\frac{\partial}{\partial t}\varphi_{l,l}(t) + 2B\,\mathrm{Re}\left\{\frac{(A_l l^2 + B_{l+1}(l+1)^2)}{2l+1}\varphi_{l,l}(t)\right.$$
$$-A_{l+1}(l+1)\frac{(l+2)(2l-1)}{(2l+1)^2}\mathrm{e}^{-\beta(E_{l+1}-E_l)}\varphi_{l+1,l+1}(t)$$
$$-B_l l\frac{(l-1)(2l+3)}{(2l+1)^2}\mathrm{e}^{\beta(E_l-E_{l-1})}\varphi_{l-1,l-1}(t)(1-\delta_{l0})$$
$$\left.-3\frac{(B_l l + A_{l+1}(l+1))}{(2l+1)^2}\mathrm{e}^{\beta(E_l-E_{l-1})}\eta_{l-1,l+1}(t)(1-\delta_{l0})\right\}$$
$$= \frac{\mu E(t)}{\hbar}\left(\frac{2l-1}{2l+1}\,\mathrm{Im}\,\sigma_{l,l+1}(t) - \mathrm{e}^{\beta(E_l-E_{l-1})}\frac{2l+3}{2l+1}\,\mathrm{Im}\,\sigma_{l-1,l}(t)(1-\delta_{l,0})\right) \quad (28)$$

and

(iii) the reduced HT3:

$$\left[\frac{\partial}{\partial t} - \frac{\mathrm{i}\hbar}{I}(2l+3)\right]\eta_{l,l+2}(t) + B\left[\left\{[A_l^* l^2 + B_{l+1}(l+1)^2]\frac{1}{2l+1}\right.\right.$$
$$\left.+[A_{l+2}(l+2)^2 + B_{l+3}^*(l+3)^2]\frac{1}{2l+5}\right\}\eta_{l,l+2}(t)$$
$$-\frac{l}{2l+1}\mathrm{e}^{\beta(E_l-E_{l-1})}[B_l^* l + B_{l+2}(l+2)]\eta_{l-1,l+1}(t)(1-\delta_{l0})$$
$$-\mathrm{e}^{-\beta(E_{l+1}-E_l)}\frac{l+3}{2l+5}[A_{l+1}^*(l+1) + A_{l+3}(l+3)]\eta_{l+1,l+3}(t)$$
$$\left.-\frac{2}{(2l+1)(2l+5)}[A_{l+1}^*(l+1) + B_{l+2}(l+2)]\varphi_{l+1,l+1}(t)\right]$$
$$= \mathrm{i}\frac{\mu E(t)}{\hbar}(\mathrm{e}^{-\beta(E_{l+1}-E_l)}\sigma_{l+1,l+2}(t) - \sigma_{l,l+1}(t)) - \mathrm{i}\frac{\Delta\alpha E(t)^2}{2\hbar}(1-\mathrm{e}^{-\beta(E_{l+2}-E_l)}) \quad (29)$$

where $\Delta\alpha = (\alpha_\parallel - \alpha_\perp)$. If the reduced HT1, HT2 and HT3 equations are solved exactly, for all l and all model parameters such as temperature T, inertial effects $B = \zeta/I$ and moderate fields, then the exact analysis of the dielectric properties of polar or polarizable fluids is accessible for a wide range of temperatures and frequencies. In the paragraph that follows, we present a low-frequency analysis of this problem. This is the classical Brownian limit which is a highly explored aspect of the problem [1, 12–14].

4. The classical Brownian limit in constant field

In the classical Brownian limit [13, 15] the bath is much faster than the rotator, in other words, the rotator frequencies $\omega_l = \hbar l/I$ are much smaller than its mean thermal agitation frequency $\omega_{\mathrm{mean}} = (k_B T/I)^{0.5}$ which in turn is much smaller than the typical oscillator frequency ω_D. The spectrum of $\hat{H}_S$ is assumed to be continuous. These hypotheses justify the following limit:

$$a = \frac{(\hbar/I)^2}{(k_B T/I)} \to 0 \qquad \text{and} \qquad \frac{k_B T}{I\omega_D^2} \to 0 \quad (30)$$

and continuum approximation

$$\frac{a}{2}l(l+1) \to x. \quad (31)$$

Transformation (31) is similar to the one used in [12, 13] on the Fokker–Planck–Kramers equation where they let $x = \frac{I\Omega^2}{2k_BT}$, where Ω is the angular velocity of the rotator.

On letting

$$\sigma_{l,l+1}(t) = \sigma_{1l}(t) + \mathrm{i}(l+1)\sigma_{2l}(t) \tag{32}$$

$$\eta_{l,l+2}(t) = \eta_{1l}(t) + \mathrm{i}(2l+3)\eta_{2l}(t) \tag{33}$$

while taking $\varphi(x,t)$, $\sigma_1(x,t)$, $\sigma_2(x,t)$, $\eta_1(x,t)$ and $\eta_2(x,t)$ to be the continuum analogues of $\varphi_{l,l}(t)$, σ_{1l}, σ_{2l}, $\eta_{1l}(t)$ and $\eta_{2l}(t)$, respectively, we obtain the system of coupled partial second-order differential equations:

$$\left[\frac{\partial}{\partial\tau} - 2\left(x\frac{\partial^2}{\partial x^2} + (1-x)\frac{\partial}{\partial x}\right)\right]\sigma_1(x,\tau) + 2b_2x\sigma_2(x,\tau) = 0 \tag{34}$$

$$\left[\frac{\partial}{\partial\tau} - 2\left(x\frac{\partial^2}{\partial x^2} + (2-x)\frac{\partial}{\partial x} - \frac{1}{2}\right)\right]\sigma_2(x,\tau) - b_1\sigma_1(x,\tau) = -b_1\frac{\mu E(\tau)}{k_BT} \tag{35}$$

$$\begin{aligned}\left[\frac{\partial}{\partial\tau} - 2\left(x\frac{\partial^2}{\partial x^2} + (1-x)\frac{\partial}{\partial x}\right)\right]\varphi(x,\tau) + \frac{3}{2x}(\varphi(x,\tau) - \eta_1(x,\tau))\\ = 2b_2\frac{\mu E(\tau)}{k_BT}\left(\frac{\partial}{\partial x} - x + 1\right)\sigma_2(x,\tau) - 3b_2\frac{\mu E(\tau)}{k_BT}\sigma_2(x,\tau)\end{aligned} \tag{36}$$

$$\begin{aligned}\left[\frac{\partial}{\partial\tau} - 2\left(x\frac{\partial^2}{\partial x^2} + (1-x)\frac{\partial}{\partial x}\right)\right]\eta_1(x,\tau) + 8b_2x\eta_2(x,\tau) - \frac{1}{2x}(\varphi(x,\tau) - \eta_1(x,\tau))\\ = -2b_2\frac{\mu E(\tau)}{k_BT}\left[\frac{\partial}{\partial x} - x + 1\right]\sigma_2(x,\tau) - 2b_2\frac{\mu E(\tau)}{k_BT}\sigma_2(x,\tau)\end{aligned} \tag{37}$$

$$\begin{aligned}\left[\frac{\partial}{\partial\tau} - 2\left(x\frac{\partial^2}{\partial x^2} + (2-x)\frac{\partial}{\partial x} - \frac{1}{2}\right)\right]\eta_2(x,\tau) - b_1\eta_1(x,\tau)\\ = \frac{b_1}{2}\frac{\mu E(\tau)}{k_BT}\left[\frac{\partial}{\partial x} - 1\right]\sigma_1(x,\tau) - b_1\frac{\Delta\alpha E(\tau)^2}{2k_BT}\end{aligned} \tag{38}$$

where $b_1 = \overline{h}/(IB)$, $b_2 = \overline{h}/(aIB)$ and $\tau = Bt$ is a dimensionless time.

4.1. The constant field susceptibility

By using the continuum approximation in equation (17) we obtain

$$P(\tau) = \frac{\mu}{3}\int_0^\infty \mathrm{d}x\, \mathrm{e}^{-x}\sigma_1(x,\tau). \tag{39}$$

Remark that the spatial parts of the differential operators defining the various functions are related to those of the generalized Laguerre polynomials $L_j^m(x)$ for $x \in [0,\infty)$. We look for solutions to the system (34), (35) in the form:

$$\begin{pmatrix}\sigma_1(x,\tau)\\ \sigma_2(x,\tau)\end{pmatrix} = \sum_{j=0}^{\infty}\begin{pmatrix}S_j^0(\tau)L_j(x)\\ S_j^1(\tau)L_j^1(x)\end{pmatrix}. \tag{40}$$

Using this together with the orthogonality property of the Laguerres in equation (39), we obtain

$$P(\tau) = \frac{\mu}{3}S_0^0(\tau). \tag{41}$$

The properties of $L_j^m(x)$ applied to equations (34) and (35) give the differential difference equations for the coefficients $S_j^0(\tau)$ and $S_j^1(\tau)$ as:

$$\left(\frac{\mathrm{d}}{\mathrm{d}\tau} + 2j\right) S_j^0(\tau) + 2b_2[(j+1)S_j^1(\tau) - jS_{j-1}^1(\tau)] = 0 \tag{42}$$

and

$$\left(\frac{\mathrm{d}}{\mathrm{d}\tau} + 2j + 1\right) S_j^1(\tau) - b_1[S_j^0(\tau) - S_{j+1}^0(\tau)] = -b_1 \frac{\mu E(\tau)}{k_B T}\delta_{j,0} \tag{43}$$

with $S_j^0(0) = S_j^1(0) = 0$. For commodity reasons, equations (41)–(43) will be referred to, in subsequent works, as the classical HT equations for the electrical polarization.

On taking the Laplace transforms of equations (41)–(43), for $E(t) = E_c$, while searching for $S_0^0(s' = s/B)$ as a continued fraction, we obtain the spectral function or the reduced susceptibility

$$\chi_r^\star(\omega') = \mathrm{i}\omega'\tilde{P}(\mathrm{i}\omega')/P(0)$$
$$= \cfrac{2\gamma}{2\gamma + \mathrm{i}\omega'(\mathrm{i}\omega'+1) + \cfrac{2\gamma\,\mathrm{i}\omega'}{\mathrm{i}\omega' + 2 + \cfrac{4\gamma}{\mathrm{i}\omega' + 3 + \cfrac{4\gamma}{s' + 4 + \cfrac{6\gamma}{\mathrm{i}\omega' + 5 + \cdots}}}}} \tag{44}$$

where $\gamma = Ik_BT/\zeta^2$. The convergence of this fraction is governed by the parameter $\gamma = (Ik_BT/\zeta^2)$. For low frequencies ($\omega' = \omega/B \ll 1$), it converges strongly. This expression, thus, explicitly describes the low-frequency spectrum of classical fluids.

Figure 1 shows the variation of the real part of the normalized complex susceptibility as a function of $\log_{10}(\omega/10^9)$ for different values of $\gamma = k_BT/(IB^2)$. For each value of this parameter, the second and fourth convergents of equation (44) are plotted. Curves $A_{2,4}$

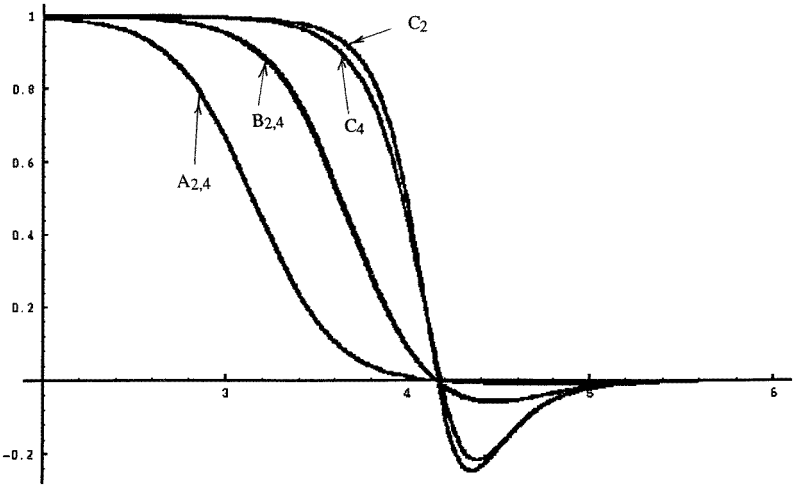

Figure 1. Plot of the real part of the normalized susceptibility versus $\log_{10}(\omega/10^9)$ for $a = \hbar^2/(Ik_BT) = 0.05$: (A) $\gamma = 0.005$, (B) $\gamma = 0.05$ and (C) $\gamma = 0.5$. Coefficients 2 and 4 in $A_{2,4}$ stand for the order of convergence of the continued fraction (44).

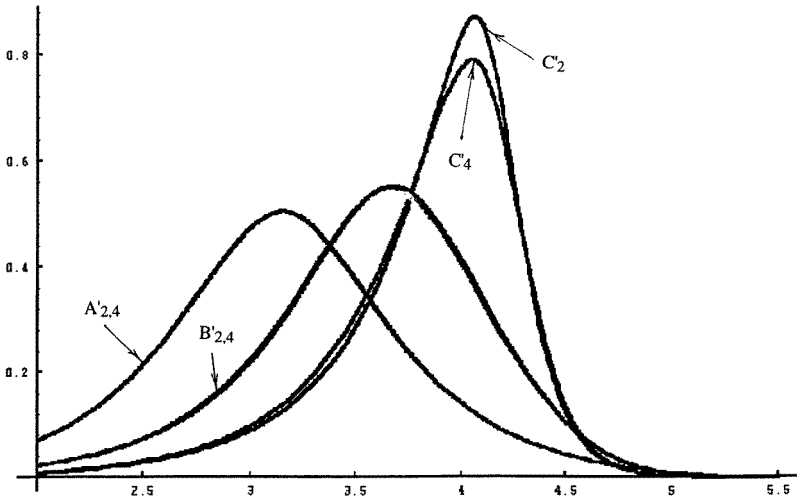

Figure 2. Plot of the imaginary part of the normalized susceptibility versus $\log_{10}(\omega/10^9)$ for $a = \hbar^2/(Ik_BT) = 0.05$: (A') $\gamma = 0.005$, (B') $\gamma = 0.05$ and (C') $\gamma = 0.5$. Coefficients 2 and 4 in $A'_{2,4}$ stand for the order of convergence of the continued fraction (44).

are the plots for $\gamma = 0.005$. A_2 and A_4 coincide exactly for the whole frequency spectrum. Similarly $B_{2,4}$ are the plots for $\gamma = 0.05$. Oncemore, the convergents coincide. Finally, C_2 and C_4 are those for $\gamma = 0.5$. They are distinct for a wide range of frequencies. Remark that all six curves present kink shapes with the kink frequency ranges and steepnesses increasing with increasing γ. The curves are drawn for a constant value of the mean thermal agitation frequency $\omega_{\text{mean}} = (k_BT/I)^{0.5} = 10^{13}$ rad s^{-1}. From $\omega \geqslant 1.6 \times 10^{13}$ rad s^{-1}, dispersion (the real part) becomes negative reaching a minimum value at a frequency of 2.5×10^{13} rad s^{-1} and increasing uniformly to zero for very high frequencies.

Figure 2 shows the imaginary part of the normalized susceptibility as a function of $\log_{10}(\omega/10^9)$. The curves $A'_{2,4}$, $B'_{2,4}$, C'_2 and C'_4 are defined in a similar manner as in figure 1. This figure illustrates exactly absorption resonance. From the curves, we remark that resonance frequencies and resonance bandwidths depend strongly on friction ζ, through $\gamma = Ik_BT/\zeta^2$. For large friction ($\gamma = 0.005$), resonance occurs at a frequency of 10^{12} rad s^{-1} with band width $\Delta\omega = 2.8 \times 10^{12}$ rad s^{-1}. For moderate friction, ($\gamma = 0.05$), it occurs at 4.5×10^{12} rad s^{-1} with a width $\Delta\omega = 1.4 \times 10^{13}$ rad s^{-1} and finally, at 1.1×10^{13} rad s^{-1} for $\gamma = 0.5$. It is important to remark that the relative positions of resonances are independent of the order of convergence of the continued fraction (44) for given value of γ, but the order influences the magnitude of the loss factor (imaginary part) and the real part of the electrical susceptibility. The convergence of the continued fraction (44) is thus, guaranteed for large frictions and/or small inertial effects.

4.2. The Kerr function

We apply the continuum approximation to equation (21) to obtain

$$\Phi(t) = \tfrac{1}{30} \int_0^\infty \mathrm{d}x\, \mathrm{e}^{-x} (\varphi(x,t) + 3\eta_1(x,t)). \tag{45}$$

On performing the change of function

$$\phi(x,t) = \varphi(x,t) + 3\eta_1(x,t) \tag{46}$$

in the system (36)–(38) and looking for solutions in the form

$$\begin{pmatrix} \varphi(x,\tau) \\ \phi(x,\tau) \\ \eta_2(x,\tau) \end{pmatrix} = \sum_{j=0}^{\infty} \begin{pmatrix} X_j(\tau)L_j(x) \\ Y_j^0(\tau)L_j(x) \\ Y_j^1(\tau)L_j^1(x) \end{pmatrix} \tag{47}$$

the Kerr function reads,

$$\Phi(\tau) = \tfrac{1}{30} Y_0^0(\tau) \tag{48}$$

and the coefficients $X_j(\tau)$, $Y_j^0(\tau)$ and $Y_j^1(\tau)$ verify the coupled differential difference equations:

$$\begin{aligned} &\left[(2j+1)\left(\frac{\mathrm{d}}{\mathrm{d}\tau}+2j\right)+2\right]X_j(\tau) - j\left(\frac{\mathrm{d}}{\mathrm{d}\tau}+2j-2\right)X_{j-1}(\tau) \\ &\qquad -(j+1)\left(\frac{\mathrm{d}}{\mathrm{d}\tau}+2j+2\right)X_{j+1}(\tau) - \frac{1}{2}Y_j^0(\tau) \\ &\qquad = b_2\frac{\mu E(\tau)}{k_B T}[-2j(j-1)S_{j-2}^1(\tau) + j(4j+5)S_{j-1}^1(\tau) - (j+1)(2j+3)S_j^1(\tau)] \end{aligned} \tag{49}$$

$$\left(\frac{\mathrm{d}}{\mathrm{d}\tau}+2j\right)Y_j^0(\tau) + 24b_2((j+1)Y_j^1(\tau) - jY_{j-1}^1(\tau)) = -4b_2\frac{\mu E(\tau)}{k_B T}S_{j-1}^1 \tag{50}$$

$$\begin{aligned} &\left(\frac{\mathrm{d}}{\mathrm{d}\tau}+2j+1\right)Y_j^1(\tau) - \frac{b_1}{3}(Y_j^0(\tau) - Y_{j+1}^0(\tau)) + \frac{b_1}{3}(X_j(\tau) - X_{j+1}(\tau)) \\ &\qquad = -b_1\frac{\mu E(\tau)}{k_B T}S_j^0 - b_1\frac{\Delta\alpha E(\tau)^2}{k_B T}\delta_{j,0}. \end{aligned} \tag{51}$$

For the same reasons as above, equations (48)–(51) will be termed the classical HT equations for the optical Kerr effect.

On solving the system (49)–(51) for Y_0^0 in the Laplace variable we obtain the Kerr function:

$$\begin{aligned} \tilde{\Phi}(s') = {} & \frac{1}{15B}\frac{(\alpha_\parallel - \alpha_\perp)E_c^2}{k_B T} \\ & \times \frac{1}{s'}\left(1 + R\cfrac{\cfrac{4\gamma}{s'+2}}{2\gamma + s'(s'+1) + \cfrac{2\gamma s'}{s'+2 + \cfrac{4\gamma}{s'+3 + \cfrac{4\gamma}{s'+4 + \cfrac{6\gamma}{s'+5+\cdots}}}}}\right) \\ & \times \cfrac{6\gamma}{s'(s'+1) + 4\gamma\frac{2s'+3}{s'+2} + \cfrac{8\gamma s'}{s'+2 + \cfrac{16\gamma}{s'+3 - \cfrac{4\gamma}{(s'+2)(s'+4)} + \cfrac{16\gamma}{s'+4 + \cfrac{24\gamma}{s'+5 - \cfrac{4\gamma}{(s'+4)(s'+6)} + \cfrac{24\gamma}{s'+6+\cdots}}}}}} \end{aligned} \tag{52}$$

with $R = \mu^2/[(\alpha_\parallel - \alpha_\perp)k_BT]$. The corresponding spectral function is

$$\Delta n^*(\omega') = \left(1 + R\,\frac{\dfrac{4\gamma}{\mathrm{i}\omega' + 2}}{2\gamma + \mathrm{i}\omega'(\mathrm{i}\omega' + 1) + \dfrac{2\gamma\,\mathrm{i}\omega'}{\mathrm{i}\omega' + 2 + \dfrac{4\gamma}{\mathrm{i}\omega' + 3 + \dfrac{4\gamma}{\mathrm{i}\omega' + 4 + \dfrac{6\gamma}{\mathrm{i}\omega' + 5 + \cdots}}}}}\right) \times \frac{6\gamma}{\mathrm{i}\omega'(\mathrm{i}\omega' + 1) + 4\gamma\,\dfrac{2\mathrm{i}\omega' + 3}{\mathrm{i}\omega' + 2} + \dfrac{8\gamma\mathrm{i}\omega'}{\mathrm{i}\omega' + 2 + \dfrac{16\gamma}{\mathrm{i}\omega' + 3 - \dfrac{4\gamma}{(\mathrm{i}\omega' + 2)(\mathrm{i}\omega' + 4)} + \dfrac{16\gamma}{\mathrm{i}\omega' + 4 + \dfrac{24\gamma}{\mathrm{i}\omega' + 5 - \dfrac{4\gamma}{(\mathrm{i}\omega' + 4)(\mathrm{i}\omega' + 6)} + \dfrac{24\gamma}{\mathrm{i}\omega' + 6 + \cdots}}}}}}. \tag{53}$$

Remark that the steady-state Kerr function [16] is recovered from equation (52) as

$$\Phi_{\mathrm{stat}} = \lim_{s' \to 0}[s' B \tilde{\Phi}(s')] = \frac{E_c^2}{15}\left(\frac{\alpha_\parallel - \alpha_\perp}{k_BT} + \left(\frac{\mu}{k_BT}\right)^2\right). \tag{54}$$

Let us point out here, the specific character of the Kerr response function which stands as a ratio of continued fractions as opposed to that of the relaxation regime [9] where it is a simple continued fraction.

Figures 3 and 4 are the plots of the real and the imaginary parts of the Kerr spectral function (53) as functions of $\log_{10}(\omega/10^9)$ for differing values of the parameter R. Curve (1) illustrates the case of highly polarizable non-polar systems ($R = 0$), (2) the case of polarizable polar systems ($R = 1$) and (3) that of highly polar ones ($R = 100$). In each case, the third convergent is considered. Note that both functions increase with increasing R.

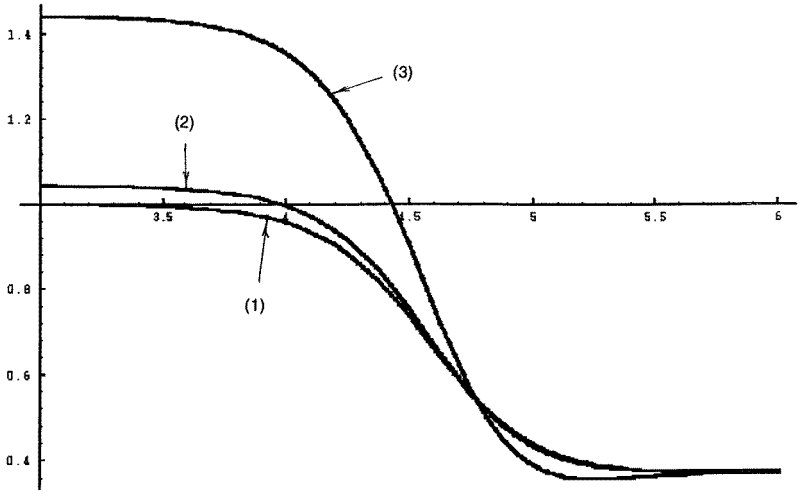

Figure 3. Plot of the real part of the normalized classical Kerr spectral function versus $\log_{10}(\omega/10^9)$ for $a = \hbar^2/(Ik_BT) = 0.05$: (1) $R = 0$, (2) $R = 1$ and (3) $R = 100$.

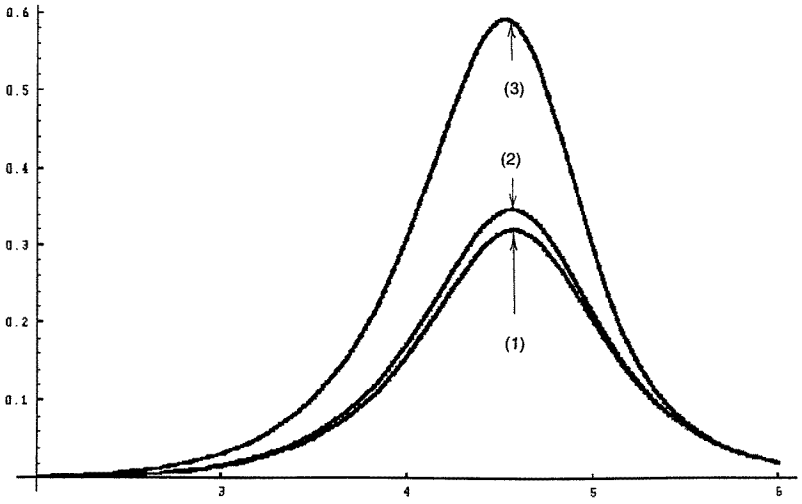

Figure 4. Plot of the imaginary part of the normalized classical Kerr spectral function versus $\log_{10}(\omega/10^9)$ for $a = \overline{h}^2/(Ik_BT) = 0.05$: (1) $R = 0$, (2) $R = 1$ and (3) $R = 100$.

5. The rotating wave approximation (RWA) limit

In this limit, we assume that the solution of the rotators in the bath is highly diluted so that the pressure and consequently friction are very low. The coupling parameter B or the characteristic rotator-bath frequency is very small compared with the rotator lines $\omega_l = (\overline{h}l/I)$. The dynamics of the rotator is virtually governed by the free rotation in the orienting field. Coupling affects only the frequency shifts and line widths.

Using a mathematical theorem on weak coupling [10, 18], all 'off-diagonal terms' and couplings between matrix elements can be ignored in equations (27)–(29) so that they become:

$$\left(\frac{\partial}{\partial t} - \mathrm{i}(\omega_{l+1} + \Delta\omega_{l+1}) + \Gamma_{l+1}\right)\sigma_{l,l+1}(t) = -\mathrm{i}\frac{\mu E(t)}{\overline{h}}(1 - \mathrm{e}^{-\beta(E_{l+1}-E_l)}) \tag{55}$$

$$\left(\frac{\partial}{\partial t} + \gamma_l\right)\varphi_{l,l}(t) = \frac{\mu E(t)}{\overline{h}}\left(\frac{2l-1}{2l+1}\,\mathrm{Im}\,\sigma_{l,l+1}(t) - \mathrm{e}^{\beta(E_l-E_{l-1})}\frac{2l+3}{2l+1}\,\mathrm{Im}\,\sigma_{l-1,l}(t)(1-\delta_{l,0})\right) \tag{56}$$

$$\left(\frac{\partial}{\partial t} - \mathrm{i}(\omega_{2l+3} + \Delta\omega_{2l+3}) + \Gamma_{2l+3}\right)\eta_{l,l+2}(t) = \mathrm{i}\frac{\mu E(t)}{\overline{h}}(\mathrm{e}^{-\beta(E_{l+1}-E_l)}\sigma_{l+1,l+2}(t) - \sigma_{l,l+1}(t)) - \mathrm{i}\frac{\Delta\alpha E(t)^2}{2\overline{h}}(1 - \mathrm{e}^{-\beta(E_{l+2}-E_l)}) \tag{57}$$

with initial conditions $\sigma_{l,l+1}(0) = \varphi_{l,l}(0) = \eta_{l,l+2}(0) = 0$. We define the dimensionless line widths and frequency shifts:

$$\gamma_l' = \frac{I}{\overline{h}}\gamma_l = \frac{2BI}{\overline{h}}\left[\frac{l^2}{2l+1}\left(1 + \frac{1}{\mathrm{e}^{\beta\overline{h}\omega_l} - 1}\right) + \frac{(l+1)^2}{\mathrm{e}^{\beta\overline{h}\omega_{l+1}} - 1}\right] \tag{58}$$

$$\Gamma_{l+1}' = \tfrac{1}{2}(\gamma_l' + \gamma_{l+1}') \tag{59}$$

$$\Gamma_{2l+3}' = \tfrac{1}{2}(\gamma_l' + \gamma_{l+2}') \tag{60}$$

$$\Delta\omega'_{l+1} = -\frac{4\overline{h}^3 B}{Ik_B^2 T^2}(2l+3)\sum_{n=0}^{\infty}\frac{(2n\pi)^3}{[(2n\pi)^2+(al)^2]} \times\frac{1}{[(2n\pi)^2+(a(l+1))^2][(2n\pi)^2+(a(l+2))^2]} \tag{61}$$

$$\Delta\omega'_{2l+3} = -\frac{4\overline{h}^3 B}{Ik_B^2 T^2}(2l+3)\sum_{n=0}^{\infty}\frac{(2n\pi)^5(1+\frac{a}{(n\pi)^2}(l^2+3l+3))}{[(2n\pi)^2+(al)^2][(2n\pi)^2+(a(l+1))^2]} \times\frac{1}{[(2n\pi)^2+(a(l+1))^2][(2n\pi)^2+(a(l+2))^2]}. \tag{62}$$

These functions well indicate how line widths and frequency shifts respond to changing physical parameters such as inertia, friction and temperature, thus their utility in exploring the influence of the parameter variations on spectral lines. Note that in our dimensionless frequency unit we define the quantum state frequency $\omega'_l = l$. Equations (17) and (55) will be called the quantum HT equations for the electrical susceptibility while (21), (56) and (57) are those of the Kerr effect. The classical and quantum HT equations for the electrical susceptibility and the Kerr optical effect so termed are very general in field type. The description of dielectric relaxation phenomena could also be done using these equations, putting in them $E(t) = 0$ and setting appropriate initial conditions.

5.1. The DC field susceptibility

In constant field, equation (55) is solved to obtain

$$\begin{aligned}\sigma_{l,l+1}(t) = {} & \frac{(\mu E_c/\overline{h})[1-\exp[-\frac{\overline{h}^2}{Ik_BT}(l+1)]]}{\Gamma_{l+1}^2+(\omega_{l+1}+\Delta\omega_{l+1})^2} \\ & \times\{(\omega_{l+1}+\Delta\omega_{l+1})[1-\mathrm{e}^{-\Gamma_{l+1}t}\cos(\omega_{l+1}+\Delta\omega_{l+1})t] \\ & -\Gamma_{l+1}\sin[(\omega_{l+1}+\Delta\omega_{l+1})t]\mathrm{e}^{-\Gamma_{l+1}t} - \mathrm{i}(\Gamma_{l+1}[1-\mathrm{e}^{-\Gamma_{l+1}t}\cos(\omega_{l+1}+\Delta\omega_{l+1})t] \\ & +(\omega_{l+1}+\Delta\omega_{l+1})\sin[(\omega_{l+1}+\Delta\omega_{l+1})t]\mathrm{e}^{-\Gamma_{l+1}t})\}. \end{aligned} \tag{63}$$

We deduce the steady-state matrix elements

$$\sigma_{l,l+1}^{st} = \frac{(\mu E_c/\overline{h})(1-\exp[-\frac{\overline{h}^2}{Ik_BT}(l+1)])}{\Gamma_{l+1}^2+(\omega_{l+1}+\Delta\omega_{l+1})^2}((\omega_{l+1}+\Delta\omega_{l+1})-\mathrm{i}\Gamma_{l+1}). \tag{64}$$

The steady-state polarization can then be calculated. It is found to be the usual $P = \mu^2 E/3k_BT$ with a friction-dependent correction which decreases proportionately as ζ^2/Ik_BT but since this result has been obtained in the limit of small friction and/or high inertia, the additional term becomes insignificant.

On defining the deviation at time t from the above steady-state value, $\Delta\sigma_{l,l+1}(t) = \sigma_{l,l+1}^{st} - \sigma_{l,l+1}(t)$, and spectral function

$$\Delta\tilde{\sigma}_{l,l+1}(\omega) = \sigma_{l,l+1}^{st} - \mathrm{i}\omega\int_0^{\infty}\Delta\sigma_{l,l+1}(t)\mathrm{e}^{-\mathrm{i}\omega t}\,\mathrm{d}t \tag{65}$$

we obtain from equation (17), the reduced susceptibility

$$\Delta\chi_r^{\star}(\omega') = \Delta\chi_r'(\omega') - \mathrm{i}\Delta\chi_r''(\omega') \tag{66}$$

where

$$\Delta\chi_r'(\omega') = \sum_{l=0}^{\infty}(l+1)(l+1+\Delta\omega'_{l+1})(\mathrm{e}^{-\beta E_l} - \mathrm{e}^{-\beta E_{l+1}})$$

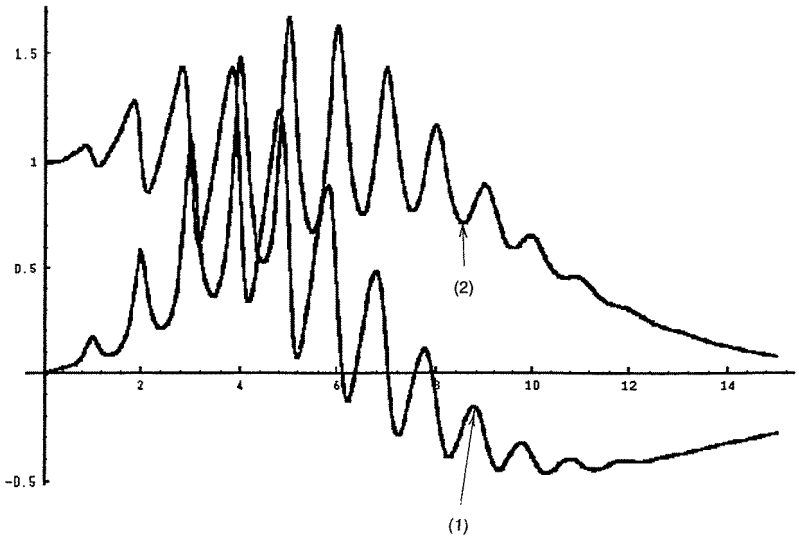

Figure 5. Plot of the real (1) and the imaginary (2) parts of normalized susceptibility versus the dimensionless frequency $\omega' = \omega/(\overline{h}/I)$ for $a = \overline{h}^2/(Ik_BT) = 0.05$, $B = 0.001\omega_{\text{mean}}$ (RWA).

$$\times \frac{(l+1+\Delta\omega'_{l+1})^2 - \omega'^2 + \Gamma'^2_{l+1}}{[(l+1+\Delta\omega'_{l+1})^2 - \omega'^2 + \Gamma'^2_{l+1}]^2 + 4\omega'^2\Gamma'^2_{l+1}} \tag{67}$$

and

$$\Delta\chi''_r(\omega') = \sum_{l=0}^{\infty} 2(l+1)(l+1+\Delta\omega'_{l+1})(\mathrm{e}^{-\beta E_l} - \mathrm{e}^{-\beta E_{l+1}}) \times \frac{\omega'\Gamma'_{l+1}}{[(l+1+\Delta\omega'_{l+1})^2 - \omega'^2 + \Gamma'^2_{l+1}]^2 + 4\omega'^2\Gamma'^2_{l+1}} \tag{68}$$

with $\omega' = \omega I/\overline{h}$.

Figure 5 shows the plots of the normalized dispersion coefficient (1) and loss factor (2) as functions of the dimensionless frequency $\omega' = \omega I/\overline{h}$ for weak coupling ($B = 10^{-3}\omega_{\text{mean}}$) with $\overline{h}^2/(Ik_BT) = 0.05$. The loss factor, an entirely positive quantity, presents an oscillatory character for $1 \leqslant \omega' \leqslant 10$ and vanishes for very high frequencies. Dispersion also shows this oscillatory behaviour but for high frequencies, it reverses sign and tends asymptotically to zero.

5.2. The Kerr function

Equations (56) and (57) give the integral form for $\varphi_{l,l}(t)$ and $\eta_{l,l+2}(t)$:

$$\varphi_{l,l}(t) = \frac{\mu E}{\overline{h}}\frac{2l-1}{2l+1}\exp(-\gamma_l t)\int_0^t \mathrm{d}t'\,\exp(\gamma_l t')\,\mathrm{Im}\,\sigma_{l,l+1}(t') - \frac{\mu E}{\overline{h}}\mathrm{e}^{-al}\frac{2l+3}{2l+1}\exp(-\gamma_l t)\int_0^t \mathrm{d}t'\,\exp(\gamma_l t')\,\mathrm{Im}\,\sigma_{l-1,l}(t') \tag{69}$$

and

$$\eta_{l,l+2}(t) = \mathrm{i}\frac{\mu E}{\overline{h}}\mathrm{e}^{-a(l+1)}\exp[-\{\Gamma_{2l+3} - \mathrm{i}(\omega_{2l+3} + \Delta\omega_{2l+3})\}t]$$

$$\times \int_0^t \mathrm{d}t' \ \exp[\{\Gamma_{2l+3} - \mathrm{i}(\omega_{2l+3} + \Delta\omega_{2l+3})\}t']\sigma_{l+1,l+2}(t')$$
$$-\mathrm{i}\frac{\mu E}{\hbar} \exp[-\{\Gamma_{2l+3} - \mathrm{i}(\omega_{2l+3} + \Delta\omega_{2l+3})\}t]$$
$$\times \int_0^t \mathrm{d}t' \ \exp[\{\Gamma_{2l+3} - \mathrm{i}(\omega_{2l+3} + \Delta\omega_{2l+3})\}t']\sigma_{l,l+1}(t')$$
$$-\mathrm{i}\frac{\Delta\alpha E_c^2}{2\hbar}(1 - \mathrm{e}^{-a(2l+3)}) \exp[-\{\Gamma_{2l+3} - \mathrm{i}(\omega_{2l+3} + \Delta\omega_{2l+3})\}t]$$
$$\times \int_0^t \mathrm{d}t' \ \exp[\{\Gamma_{2l+3} - \mathrm{i}(\omega_{2l+3} + \Delta\omega_{2l+3})\}t'] \tag{70}$$

where $a = \hbar^2/(Ik_BT)$. When substituting for $\sigma_{l,l+1}$ as obtained previously, we easily show that

$$\varphi_{l,l}(t) = \varphi_{l,l}^{st} - \Delta\varphi_{l,l}(t) \tag{71}$$

with

$$\varphi_{l,l}^{st} = \frac{\mu^2 E^2}{\hbar^2} \mathrm{Re}\left[\frac{\frac{2l+3}{2l+1}(\mathrm{e}^{al} - 1)}{\gamma_l[\Gamma_l + \mathrm{i}(\omega_l + \Delta\omega_l)]} - \frac{\frac{2l-1}{2l+1}(1 - \mathrm{e}^{-a(l+1)})}{\gamma_l[\Gamma_{l+1} + \mathrm{i}(\omega_{l+1} + \Delta\omega_{l+1})]}\right] \tag{72}$$

and

$$\Delta\varphi_{l,l}(t) = \frac{\mu^2 E^2}{\hbar^2} \mathrm{Re}\left[\left\{\frac{2l+3}{2l+1}(\mathrm{e}^{al} - 1)\frac{1}{\gamma_l[\Gamma_l + \mathrm{i}(\omega_l + \Delta\omega_l)]}\right.\right.$$
$$\left.-\frac{2l-1}{2l+1}(1 - \mathrm{e}^{-a(l+1)})\frac{1}{\gamma_l[\Gamma_{l+1} + \mathrm{i}(\omega_{l+1} + \Delta\omega_{l+1})]}\right\} \exp(-\gamma_l t)$$
$$+\frac{2l+3}{2l+1}(\mathrm{e}^{al} - 1)\frac{\exp[-(\Gamma_l + \mathrm{i}(\omega_l + \Delta\omega_l))t]}{[\gamma_l - \Gamma_l - \mathrm{i}(\omega_l + \Delta\omega_l)][\Gamma_l + \mathrm{i}(\omega_l + \Delta\omega_l)]}$$
$$-\frac{2l-1}{2l+1}(1 - \mathrm{e}^{-a(l+1)})$$
$$\left.\times\frac{\exp[-\{\Gamma_{l+1} + \mathrm{i}(\omega_{l+1} + \Delta\omega_{l+1})\}t]}{[\gamma_l - \Gamma_{l+1} - \mathrm{i}(\omega_{l+1} - \Delta\omega_{l+1})][\Gamma_{l+1} + \mathrm{i}(\omega_{l+1} + \Delta\omega_{l+1})]}\right]. \tag{73}$$

Similarly,

$$\Delta\eta_{l,l+2}(t) = \eta_{l,l+2}^{st} - \eta_{l,l+2}(t) = \frac{\mu^2 E^2}{\hbar^2}\left[\left(\frac{1 - \mathrm{e}^{-a(l+1)}}{\Gamma_{2l+3} - \Gamma_{l+1} - \mathrm{i}(\omega_{l+2} + \Delta\omega_{l+2})}\right.\right.$$
$$\left.-\frac{\mathrm{e}^{-a(l+1)}(1 - \mathrm{e}^{-a(l+2)})}{\Gamma_{2l+3} - \Gamma_{l+2} - \mathrm{i}(\omega_{l+1} + \Delta\omega_{l+1})} - \frac{\mathrm{i}}{R}(1 - \mathrm{e}^{-a(2l+3)})\right)$$
$$\times\frac{\exp[-\{\Gamma_{2l+3} - \mathrm{i}(\omega_{2l+3} + \Delta\omega_{2l+3})\}t]}{[\Gamma_{2l+3} - \mathrm{i}(\omega_{2l+3} + \Delta\omega_{2l+3})]}$$
$$-(1 - \mathrm{e}^{-a(l+1)})\frac{\exp[-\{\Gamma_{l+1} - \mathrm{i}(\omega_{l+1} + \Delta\omega_{l+1})\}t]}{[\Gamma_{l+1} - \mathrm{i}(\omega_{l+1} + \Delta\omega_{l+1})][\Gamma_{2l+3} - \Gamma_{l+1} - \mathrm{i}(\omega_{l+2} + \Delta\omega_{l+2})]}$$
$$\left.+\frac{\mathrm{e}^{-a(l+1)}(1 - \mathrm{e}^{-a(l+2)})\exp[-\{\Gamma_{l+2} - \mathrm{i}(\omega_{l+2} + \Delta\omega_{l+2})\}t]}{[\Gamma_{l+2} - \mathrm{i}(\omega_{l+2} + \Delta\omega_{l+2})][\Gamma_{2l+3} - \Gamma_{l+2} - \mathrm{i}(\omega_{l+1} + \Delta\omega_{l+1})]}\right] \tag{74}$$

with

$$\eta_{l,l+2}^{st} = \frac{\mu^2 E^2}{\hbar^2}\left(\frac{(1 - \mathrm{e}^{-a(l+2)})\mathrm{e}^{-a(l+1)}}{\Gamma_{l+2} - \mathrm{i}(\omega_{l+2} + \Delta\omega_{l+2})} - \frac{(1 - \mathrm{e}^{-a(l+1)})}{\Gamma_{l+1} - \mathrm{i}(\omega_{l+1} + \Delta\omega_{l+1})} - \frac{\mathrm{i}}{R}(1 - \mathrm{e}^{-a(l+2)})\right)$$
$$\times\frac{1}{\Gamma_{2l+3} - \mathrm{i}(\omega_{2l+3} + \Delta\omega_{2l+3})}. \tag{75}$$

On defining a spectral function similar to that of the polarization, for all frequency $\omega = (\hbar/I)\omega'$, we obtain, after using equation (21), that

$$\Delta\tilde{\Phi}^{*}(\omega') = \Delta\tilde{\Phi}'(\omega') - \Delta\tilde{\Phi}''(\omega'). \tag{76}$$

It is important to give a physical meaning to $\Delta\tilde{\Phi}(\omega')$. Its time picture depicts the deviation at time t from its steady-state value $\frac{E^2}{15}((\mu/k_BT)^2 + (\Delta\alpha/k_BT))$. $\Delta\Phi(t)$ therefore describes the transient state following the sudden application of the constant electric field. It can also be called a relaxation function. Using its spectral function observed spectra may be accounted for. This method of characterizing dielectrics should be capable of recovering results furnished by the field removal relaxation method [9, 10]. On the other hand, some new important features will appear. The field removal relaxation reveals only one type of rotational transition ($l \to l+2$) but due to the fact that the new approach couples both susceptibility and the Kerr function (cf equations (27)–(29)), $l \to l+1$ also intervene in the relaxation mechanism. This method is therefore important as spectral lines not accounted for by the the usual method appear naturally.

Regardless of the complicated mathematical form of the real and the imaginary parts of this function, their significance for the interpretation of relevant physical properties of dielectric media earns them being written out explicitly as:

$$\begin{aligned}
\Delta\tilde{\Phi}'(\omega') = \frac{1}{15}\left(\frac{\mu E_c}{k_BT}\right)^2 \sum_{l=0}^{\infty} \frac{l+1}{a(2l+3)} \mathrm{e}^{-\beta E_l} \\
\times\Bigg\{ -l(1-\mathrm{e}^{-a(l+1)})\gamma_l'\Gamma_{l+1}' \Big/ [(\Gamma_{l+1}'^2 + (l+1+\Delta\omega_{l+1}')^2)(\gamma_l'^2+\omega'^2)] \\
+\frac{l(2l+3)}{2l-1}(\mathrm{e}^{al}-1)\gamma_l'\Gamma_l' \Big/ [(\Gamma_l'^2 + (l+\Delta\omega_l')^2)(\gamma_l'^2+\omega'^2)] \\
-l(1-\mathrm{e}^{-a(l+1)})\{[\Gamma_{l+1}'(\gamma_l'-\Gamma_{l+1}') + (l+1+\Delta\omega_{l+1}')^2] \\
\times[\Gamma_{l+1}'^2 + (l+1+\Delta\omega_{l+1}')^2 - \omega'^2] + 2\omega'^2\Gamma_{l+1}'(\gamma_l'-\Gamma_{l+1}')\} \\
\Big/ [\{(\gamma_l'-\Gamma_{l+1}')^2 + (l+1+\Delta\omega_{l+1}')^2\} \\
\times\{(\Gamma_{l+1}'^2 + (l+1+\Delta\omega_{l+1}')^2 - \omega'^2)^2 + 4\omega'^2\Gamma_{l+1}'^2\}] \\
+\frac{l(2l+3)}{(2l-1)}(\mathrm{e}^{al}-1)\{[\Gamma_l'(\gamma_l'-\Gamma_l') + (l+\Delta\omega_l')^2] \\
\times[\Gamma_l'^2 + (l+\Delta\omega_l')^2 - \omega'^2] + 2\omega'^2\Gamma_l'(\gamma_l'-\Gamma_l')\} \\
\Big/ [\{(\gamma_l'-\Gamma_l')^2 + (l+\Delta\omega_l')^2\}\{(\Gamma_l'^2 + (l+\Delta\omega_l')^2 - \omega'^2)^2 + 4\omega'^2\Gamma_l'^2\}] \\
-3(l+2)(1-\mathrm{e}^{-a(l+2)})\mathrm{e}^{-a(l+1)} \\
\times\{[(\Gamma_{2l+3}'-\Gamma_{l+2}')\Gamma_{2l+3} - (2l+3+\Delta\omega_{2l+3}')(l+1+\Delta\omega_{l+1}')] \\
\times[\Gamma_{2l+3}'^2 + (2l+3+\Delta\omega_{2l+3}')^2 - \omega'^2] + 2\omega'^2\Gamma_{2l+3}'(\Gamma_{2l+3}'-\Gamma_{l+2}')\} \\
\Big/ [\{(\Gamma_{2l+3}'-\Gamma_{l+2}')^2 + (l+1+\Delta\omega_{l+1}')^2\} \\
\times\{(\Gamma_{2l+3}'^2 + (2l+3+\Delta\omega_{2l+3}')^2 - \omega'^2)^2 + 4\omega'^2\Gamma_{2l+3}'^2\}] \\
+3(l+2)(1-\mathrm{e}^{-a(l+1)}) \\
\{[(\Gamma_{2l+3}'-\Gamma_{l+1})\Gamma_{2l+3} - (2l+3+\Delta\omega_{2l+3}')(l+2+\Delta\omega_{l+2}')] \\
\times[\Gamma_{2l+3}'^2 + (2l+3+\Delta\omega_{2l+3}')^2 - \omega'^2] + 2\omega'^2\Gamma_{2l+3}'(\Gamma_{2l+3}'-\Gamma_{l+1}')\}
\end{aligned}$$

$$
\begin{aligned}
&\Big/[\{(\Gamma'_{2l+3}-\Gamma'_{l+1})^2+(l+2+\Delta\omega'_{l+2})^2\}\\
&\times\{(\Gamma'^2_{2l+3}+(2l+3+\Delta\omega'_{2l+3})^2-\omega'^2)^2+4\omega'^2\Gamma'^2_{2l+3}\}]\\
&-3(l+2)(1-\mathrm{e}^{-a(l+1)})\\
&\times\{[(\Gamma'_{2l+3}-\Gamma_{l+1})\Gamma_{l+1}-(l+2+\Delta\omega'_{l+2})(l+1+\Delta\omega'_{l+1})]\\
&\times[\Gamma'^2_{l+1}+(l+1+\Delta\omega'_{l+1})^2-\omega'^2]+2\omega'^2\Gamma'_{l+1}(\Gamma'_{2l+3}-\Gamma'_{l+1})\}\\
&\Big/[\{(\Gamma'_{2l+3}-\Gamma'_{l+1})^2+(l+2+\Delta\omega'_{l+2})^2\}\\
&\times\{(\Gamma'^2_{l+1}+(l+1+\Delta\omega'_{l+1})^2-\omega'^2)^2+4\omega'^2\Gamma'^2_{l+1}\}]\\
&+3(l+2)(1-\mathrm{e}^{-a(l+2)})\mathrm{e}^{-a(l+1)}\\
&\times\{[(\Gamma'_{2l+3}-\Gamma_{l+2})\Gamma_{l+2}-(l+1+\Delta\omega'_{l+1})(l+2+\Delta\omega'_{l+2})]\\
&\times[\Gamma'^2_{l+2}+(l+2+\Delta\omega'_{l+2})^2-\omega'^2]+2\omega'^2\Gamma'_{l+2}(\Gamma'_{2l+3}-\Gamma'_{l+2})\}\\
&\Big/[\{(\Gamma'_{2l+3}-\Gamma'_{l+2})^2+(l+1+\Delta\omega'_{l+1})^2\}\\
&\times\{(\Gamma'^2_{l+2}+(l+2+\Delta\omega'_{l+2})^2-\omega'^2)^2+4\omega'^2\Gamma'^2_{l+2}\}]\\
&+\frac{3}{R}(l+2)(1-\mathrm{e}^{-a(2l+3)})[\Gamma'^2_{2l+3}+(2l+3+\Delta\omega'_{2l+3})^2-\omega'^2]\\
&\Big/[(\Gamma'^2_{2l+3}+(2l+3+\Delta\omega'_{2l+3})^2-\omega'^2)^2+4\omega'^2\Gamma'^2_{2l+3}]\Big\}
\end{aligned}
\tag{77}
$$

and

$$
\begin{aligned}
\Delta\tilde{\Phi}''(\omega')=\frac{1}{15}\left(\frac{\mu E_c}{k_BT}\right)^2\sum_{l=0}^{\infty}\frac{(l+1)\omega'}{a(2l+3)}\mathrm{e}^{-\beta E_l}&\\
\times\Big\{-l(1-\mathrm{e}^{-a(l+1)})\Gamma'_{l+1}&\Big/[\{\Gamma'^2_{l+1}+(l+1+\Delta\omega'_{l+1})^2\}(\gamma_l'^2+\omega'^2)]\\
+\frac{l(2l+3)}{2l-1}(\mathrm{e}^{al}-1)\Gamma'_l&\Big/[\{\Gamma'^2_l+(l+\Delta\omega'_l)^2\}(\gamma_l'^2+\omega'^2)]\\
-l(1-\mathrm{e}^{-a(l+1)})&\{2\Gamma'_{l+1}[(\gamma'_l-\Gamma'_{l+1})\Gamma'_{l+1}+(l+1+\Delta\omega'_{l+1})^2]\\
-(\gamma'_l-\Gamma'_{l+1})&[\Gamma'^2_{l+1}+(l+1+\Delta\omega'_{l+1})^2-\omega'^2]\}\\
&\Big/[\{(\gamma'_l-\Gamma'_{l+1})^2+(l+1+\Delta\omega'_{l+1})^2\}\\
&\times\{(\Gamma'^2_{l+1}+(l+1+\Delta\omega'_{l+1})^2-\omega'^2)^2+4\omega'^2\Gamma'^2_{l+1}\}]\\
+\frac{l(2l+3)}{(2l-1)}(\mathrm{e}^{al}-1)&\{2\Gamma'_l[(\gamma'_l-\Gamma'_l)\Gamma'_l+(l+\Delta\omega'_l)^2]\\
-(\gamma'_l-\Gamma'_l)&[\Gamma'^2_l+(l+\Delta\omega'_l)^2-\omega'^2]\}\\
&\Big/[\{(\gamma'_l-\Gamma'_l)^2+(l+\Delta\omega'_l)^2\}\{(\Gamma'^2_l+(l+\Delta\omega'_l)^2-\omega'^2)^2+4\omega'^2\Gamma'^2_l\}]\\
-3(l+2)(1-\mathrm{e}^{-a(l+2)})&\mathrm{e}^{-a(l+1)}\\
\times\{2\Gamma_{2l+3}[(\Gamma'_{2l+3}-\Gamma'_{l+2})&\Gamma_{2l+3}-(2l+3+\Delta\omega'_{2l+3})(l+1+\Delta\omega'_{l+1})]\\
-(\Gamma'_{2l+3}-\Gamma'_{l+2})&[(2l+3+\Delta\omega'_{2l+3})^2-\omega'^2+\Gamma'^2_{2l+3}]\}
\end{aligned}
$$

$$
\begin{aligned}
&\Big/[\{(\Gamma'_{2l+3}-\Gamma'_{l+2})^{+}(l+1+\Delta\omega'_{l+1})^2\}\\
&\times\{(\Gamma'^2_{2l+3}+(2l+3+\Delta\omega'_{2l+3})^2-\omega'^2)^2+4\omega'^2\Gamma'^2_{2l+3}\}]\\
&+3(l+2)(1-\mathrm{e}^{-a(l+1)})\\
&\times\{2\Gamma_{2l+3}[(\Gamma'_{2l+3}-\Gamma'_{l+1})\Gamma'_{2l+3}-(2l+3+\Delta\omega'_{2l+3})(l+2+\Delta\omega'_{l+2})]\\
&-(\Gamma'_{2l+3}-\Gamma'_{l+1})[\Gamma'^2_{2l+3}-\omega'^2+\Gamma'^2_{2l+3}]\}\\
&\Big/[\{(\Gamma'_{2l+3}-\Gamma'_{l+1})^2+(l+2+\Delta\omega'_{l+2})^2\}\\
&\times\{(\Gamma'^2_{2l+3}+(2l+3+\Delta\omega'_{2l+3})^2-\omega'^2)^2+4\omega'^2\Gamma'^2_{2l+3}\}](1-\mathrm{e}^{-a(l+1)})\\
&\times\{2\Gamma_{l+1}[(\Gamma'_{2l+3}-\Gamma'_{l+1})\Gamma_{l+1}-(l+2+\Delta\omega'_{l+2})(l+1+\Delta\omega'_{l+1})]\\
&-(\Gamma'_{2l+3}-\Gamma'_{l+1})[\Gamma'^2_{l+1}-\omega'^2+(l+1+\Delta\omega'_{l+1})^2]\}\\
&\Big/[\{(\Gamma'_{2l+3}-\Gamma'_{l+1})^2+(l+2+\Delta\omega'_{l+2})^2\}\\
&\times\{(\Gamma'^2_{l+1}+(l+1+\Delta\omega'_{l+1})^2-\omega'^2)^2+4\omega'^2\Gamma'^2_{l+1}\}]\\
&+3(l+2)(1-\mathrm{e}^{-a(l+2)})\mathrm{e}^{-a(l+1)}\\
&\times\{2\Gamma_{l+2}[(\Gamma'_{2l+3}-\Gamma'_{l+2})\Gamma'_{l+2}-(l+1+\Delta\omega'_{l+1})(l+2+\Delta\omega'_{l+2})]\\
&-(\Gamma'_{2l+3}-\Gamma'_{l+2})[\Gamma'^2_{l+2}-\omega'^2+(l+2+\Delta\omega'_{l+2})^2]\}\\
&\Big/[\{(\Gamma'_{2l+3}-\Gamma'_{l+2})^2+(l+2+\Delta\omega'_{l+2})^2\}\\
&\times\{(\Gamma'^2_{l+2}+(l+1+\Delta\omega'_{l+1})^2-\omega'^2)^2+4\omega'^2\Gamma'^2_{l+2}\}]\\
&+\frac{6}{R}(l+2)(1-\mathrm{e}^{-a(2l+3)})\Gamma'_{2l+3}\\
&\Big/[(\Gamma'^2_{2l+3}+(2l+3+\Delta\omega'_{2l+3})^2-\omega'^2)^2+4\omega'^2\Gamma'^2_{2l+3}]\Big\}
\end{aligned}
\tag{78}
$$

where $R=\mu^2/(\Delta\alpha k_BT)$. Despite a number of publications giving theoretical description of polar fluids, the problem of formulating analytical description of relevant spectra over a wide frequency range has not yet been solved. The above expressions, explicitly reveal a detailed dependence on temperature and inertial effects through the shifts and widths and could directly be exploited to analyse observed spectra and give valuable information about molecular structure, intermolecular interactions and characteristic times of molecular rotational motions.

6. Discussions

(i) Figure 1 is the normalized plot of the classical dispersion factor (the real part of the complex susceptibility) versus $\log_{10}(\omega/10^9)$ for $a=\hbar^2/(Ik_BT)=0.05$: (A) $\gamma=0.005$, (B) $\gamma=0.05$ and (C) $\gamma=0.5$. Coefficients 2 and 4 in $A_{2,4}$ stand for the order of convergence of the continued fraction (44). From this figure, we observe that the dispersion factor vanishes at same frequency ($\omega_c=1.6\times10^{13}$ rad s^{-1}) for all γ values. The more γ increases, the more the dispersion factor kink gets strong but tends asymptotically to a limit form that presents a square wall at the upper part (*y-positive*) and a sharp concavity at the bottom (*y-negative*). The well depth appearing at the bottom is the more important, the more γ increases. This phenomenon could be interpreted from the molecular structure of

the medium. Indeed, large γ values ($\gamma \geqslant 0.5$) correspond to small friction (ζ) for which the bath of oscillators is less concentrated. Collisions between the rotator and bath oscillators are less frequent, thus the bath-rotator system is less dispersive. Dispersion, then, changes very little over a wide frequency range ($0 - 4 \times 10^{12}$ rad s^{-1}) but falls abruptly to zero at a cut-off frequency equal to ω_c. In contrast to the case of large γ, small γ ($\gamma \leqslant 0.005$) correspond to large friction ζ, that means a highly concentrated bath, giving the medium a more dispersive character. Dispersion, thus, varies conspicuously with increasing frequency up to ω_c. ω_c is, thus, the frequency beyond which every medium becomes less dispersive than the vacuum. On limiting the analysis to the electrical susceptibility, therefore, all media are transparent to electromagnetic waves of frequency far above the cut-off frequency. The less concentrated the bath is, the more reduced its dispersivity is (the deeper the well).

(ii) Absorption resonance frequencies as well as its maxima increase with increasing γ. Free particles absorb radiations more than bound ones. This explains the observation that less dense media will absorb more than denser ones (see figure 2). Quantum effects start appearing when the medium characteristic frequency is of the order of $\overline{h}/I \sim 10^{13}$ rad s^{-1}. This effect manifests for weak couplings (the RWA) which here correspond to small friction (or large γ). This explains why as γ increases, resonance frequencies grow, approaching the quantum range.

(iii) For the same bath concentration ($\gamma = 0.05$):

(a) for same R values (polar or non-polar molecules), there exists an initial frequency range over which the refraction coefficient remains constant (see figure 3). This widens as the dipole moment of the molecules increases. For example, for non-polar molecules ($R = 0$), this range length is of the order 3×10^{12} rad s^{-1} while for molecules with equal permanent and induced moment energy contribution ($R = 1$), it is 6.3×10^{12} rad s^{-1} and for purely polar ones ($R \to \infty$), it stands at about 10^{13} rad s^{-1};

(b) a steady-state value of the refraction coefficient is practically attained at a frequency of 5.0×10^{14} rad s^{-1} independent of the degree of polarization of the molecules;

(c) there exists a specific frequency characterizing the bath structure at which, regardless of the molecular electronic structure, the Kerr refraction coefficient is always the same. It occurs at 6.3×10^{13} rad s^{-1} for $\gamma = 0.05$. At this frequency the Kerr absorption maxima appear which are more pronounced and therefore the more polar the molecules are.

A general view of the Kerr classical dispersion spectrum is a sluggish variation for low frequencies $0 < \omega < 10^{13}$ rad s^{-1}, followed by abrupt falls for frequencies between 10^{13} and 10^{14} rad s^{-1}. Above this value, it attains a steady positive value of 0.4 in the normalized units (see figure 3). The quantum one starts with a small constant negative value (for molecules with $\overline{h}/I \sim 4 \times 10^{12}$ rad s^{-1}, e.g. HCl) for frequencies lower than 10^{13} rad s^{-1} (for less polar systems) and beyond this frequency value spectral lines start appearing (see figures 7 and 8(1)).

(iv) For the fixed inertia/temperature parameter ($a = \overline{h}^2/\left(Ik_BT\right) = 0.05$), we observe, as the coupling parameter $s = B/\omega_{\text{mean}}$ (with $\omega_{\text{mean}}^2 = k_BT/I$) decreases from 5.0×10^{-3} through 2.5×10^{-3} to 1.0×10^{-3}, a transition from a continuous spectrum (1) through broadened lines (2) to separate lineforms (3) (see figure 6). This phenomenon was observed experimentally by Frenkel [17] for HCl in argon while varying argon density. Indeed, the line width at half height varies proportionately with the friction parameter B as potrayed by equation (58). As B increases, thus, lines broaden out and fuse up forming a continuous spectrum. This explains the fact that when B for a medium approaches ω_{mean}, the latter acquires typical classical behaviours. In contrast, when B is very small compared with ω_{mean}, particles are far apart, colliding less frequently leading to highly uncorrelated collisions. This results in pure discrete spectra. Let us make note of the fact that the

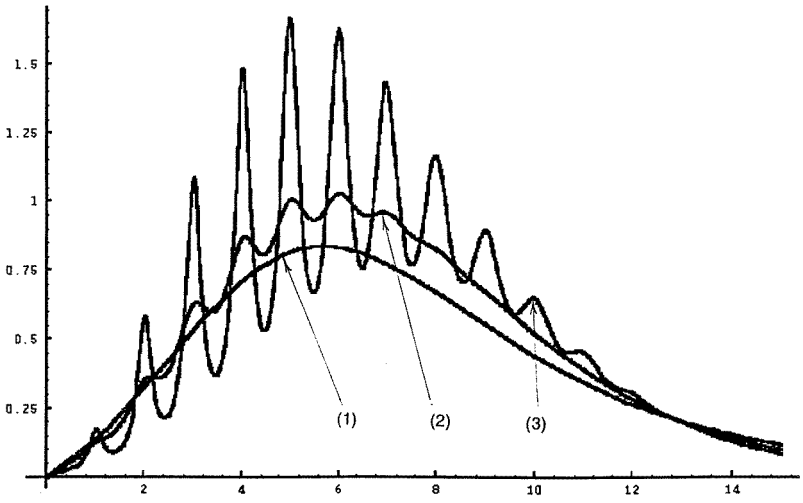

Figure 6. Plot of the imaginary part of normalized susceptibility versus the dimensionless frequency $\omega' = \omega/(\hbar/I)$ for $a = \hbar^2/(Ik_BT) = 0.05$: (1) $B = 0.0025\omega_{\text{mean}}$, (2) $B = 0.0050\omega_{\text{mean}}$ and (3) $B = 0.0010\omega_{\text{mean}}$ (RWA).

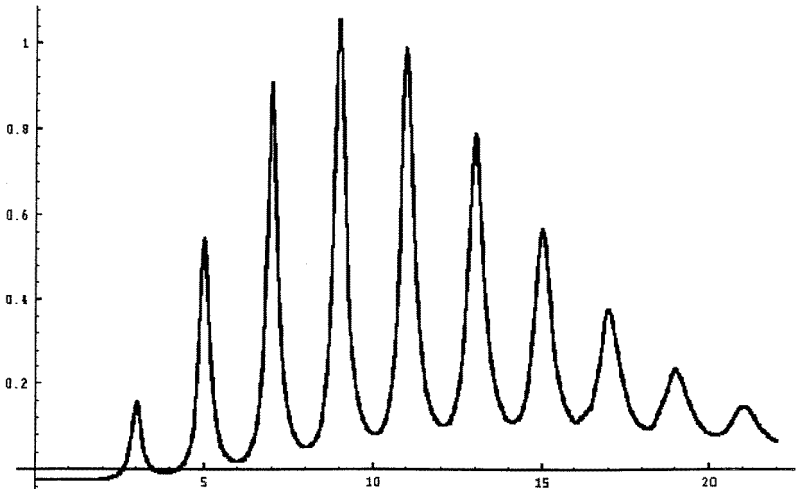

Figure 7. Plot of the real part of normalized Kerr spectral function versus the dimensionless frequency $\omega' = \omega/(\hbar/I)$ for $a = \hbar^2/(Ik_BT) = 0.05$, $R = 0$ and $B = 0.001\omega_{\text{mean}}$ (RWA).

calculated line shifts (equation (61)) have negligible influence on the spectral line positions ($\Delta\omega'_{l+1} \sim -10^{-4}(2l+3)$ as opposed to $\omega'_{l+1} = l+1$). This was also observed by Frenkel using impact cross section calculations.

(v) For the same friction parameter $B = \zeta/I = 0.001(k_BT/I)^{0.5}$, for $a = 0.05$ and for $R \neq 0$, the Kerr spectra present distorsions with amplitudes increasing with increasing R (see figures 8(2) and 10(2)). For non-polar systems, the imaginary part of the Kerr spectral function shows the usual line shape (see figure 9), meanwhile for polar ones lines start with very pronounced peaks, then falling into weak negative value peaks which vanish for large frequencies (see figure 10).

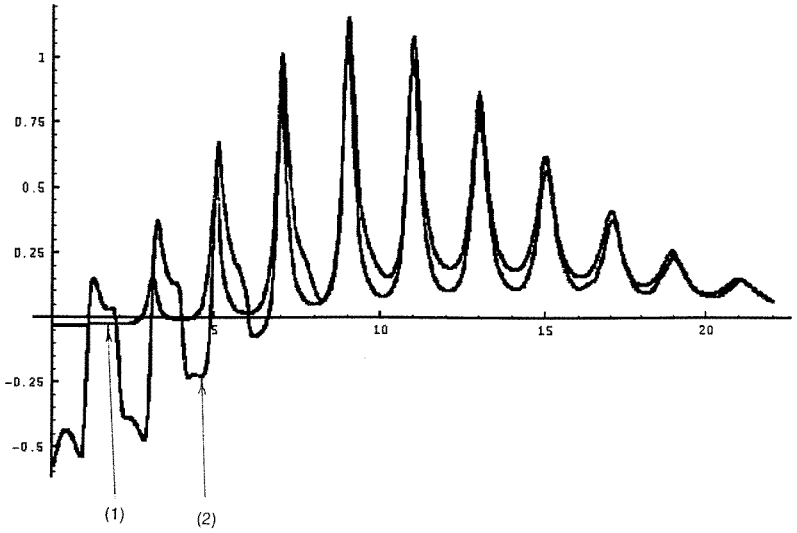

Figure 8. Plot of the real part of normalized Kerr spectral function versus the dimensionless frequency $\omega' = \omega/(\overline{h}/I)$ for $a = \overline{h}^2/(Ik_BT) = 0.05$, $B = 0.001\omega_{\text{mean}}$: (1) $R = 1$ and (2) $R = 100$ (RWA). y-units are the same as in figure 7.

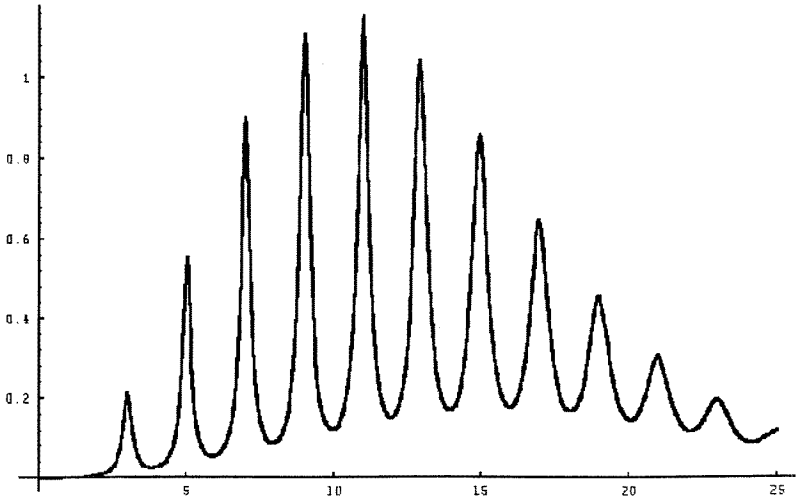

Figure 9. Plot of the imaginary part of normalized Kerr spectral function versus the dimensionless frequency $\omega' = \omega/(\overline{h}/I)$ for $a = \overline{h}^2/(Ik_BT) = 0.05$, $R = 0$ and $B = 0.001\omega_{\text{mean}}$ (RWA).

The distorsions observed in the Kerr low-frequency dispersion spectrum of polar fluids result from the mixing of lines corresponding to transitions between small quantum number l levels. Remark that, while the electrical susceptibility allows only lines corresponding to the selection rule $\Delta l = l_f - l_i = \pm 1$, to be computed, the Kerr effect accounts for transitions of the form $\Delta l = l_f - l_i = \pm 2$.

We have theoretically investigated the effect of bath concentration or friction on observed spectra of polar fluids. Bath concentration considerably affects the shape (linewidth) and

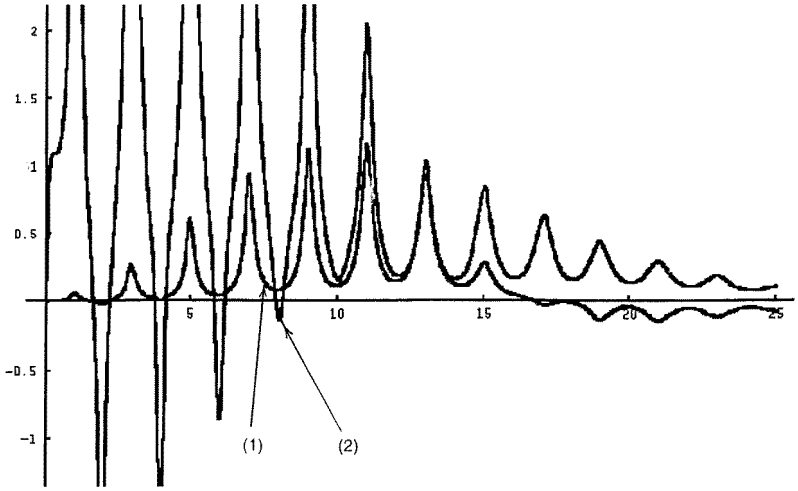

Figure 10. Plot of the imaginary part of normalized Kerr spectral function versus the dimensionless frequency $\omega' = \omega/(\overline{h}/I)$ for $a = \overline{h}^2/(Ik_BT) = 0.05$, $B = 0.001\omega_{\text{mean}}$: (1) $R = 1$ and (2) $R = 100$ (RWA).

line position of spectra. The classical continuous ones, observable for low-frequency ranges, have been highlighted while far infrared line have been analysed for less concentrated host bath. Our theory allows the exploration of the spectra of polar fluids over a wide range of temperatures and frequencies.

References

[1] Gaiduk V I and Kalmykov Yu P 1987 *J. Mol. Liq.* **34** 1
[2] Kalmykov Y P and Titov S V 1994 A semi-classical theory of dielectric relaxation and absorption: memory function approach to extended diffusion models of molecular reorientation in fluids *Relaxation Phenomena in Condensed Matter (Adv. Chem. Phys. LXXXVII)* ed W Coffey p 31
[3] Kubo R 1957 *J. Phys. Soc. Japan* **12** 570
[4] Karplus R and Schwinger J 1948 *Phys. Rev.* **74** 1020
[5] Gross E P 1955 *J. Chem. Phys.* **23** 1415
[6] Gross E P and Lebowitz J L 1956 *Phys. Rev.* **104** 1528
[7] O'Dwyer J J and Harting E 1967 *Prog. Diel.* **71**
[8] mc Clung R E D 1977 *Adv. Mol. Relaxation Interact. Process* **10** 83
[9] Titantah J T and Hounkonnou M N 1997 *J. Phys. A: Math. Gen.* **30** 6327
[10] Navez P and Hounkonnou M N 1995 *J. Phys. A: Math. Gen.* **28** 6345
[11] Morita A and Watanabe H 1979 *J. Chem. Phys.* **70** 4708
[12] Hounkonnou M N, Ronveaux A and Navez P 1994 *J. Phys. A: Math. Gen.* **27** 6635
[13] Navez P and Hounkonnou M N 1994 *J. Phys. A: Math. Gen.* **27** 6657
[14] Kalmykov Y P and Quinn K P 1991 *J. Chem. Phys.* **95** 9142
[15] Spohn H 1980 *Rev. Mod. Phys.* **53** 569
[16] Doi M and Edwards S F 1986 *The Theory of Polymer Dynamics* (Oxford: Clarendon)
[17] Frenkel D 1977 Rotational relaxation of linear rigid molecules in dense noble gases *Thesis of Doctorat ès Sciences* Universiteit van Amsterdam, Netherlands
[18] Davies E B 1976 *Math. Ann.* **219** 147